6-2015

CFD Modeling of the Flow of Resin into a Preform Mold of Carbon Fibers

Caelan Lapointe
Union College - Schenectady, NY

CFD Modeling of the Flow of Resin into a Preform Mold of Carbon Fibers

By

Caelan Lapointe

****

Submitted in partial fulfillment
of the requirements for
Honors in the Department of Mechanical Engineering

UNION COLLEGE

June, 2015

Abstract

LAPOINTE, CAELAN. CFD modeling of the flow of resin ino a preform mold of Carbon Fibers. Department of Mechanical Engineering, June 2015.

ADVISOR: Ronald B. Bucinell, Ph.D., PE

Sandwich structures are formed by separating load bearing face sheets with a light weight core material. This type of structural design is both strong and light, making for an extremely efficient structure. Sustainable sandwich structures made using face sheets of natural fiber mats and natural oil based resins separated by a fungal mycelia core. The vacuum infusion of resin into the fiber mats is investigated numerically using Star CCM+, a computational fluid dynamics (CFD) package. The methodology focuses on ease of use while emphasizing good modeling practices. The models generated are compared to the experimental results and provide a theoretical foundation for mold geometries conducive to even resin infusion.

Table of Contents

List of Tables and Figures

List of Tables:

List of Figures:

List of Variables

1. f	Body Force
2. k	Permeability Tensor
3. L	Characteristic Length
4. p	Pressure
5. P_v	Viscous Resistance Coefficient
6. P_i	Inertial Resistance Coefficient
7. q	Flow Flux
8. Re	Reynold's Number
9. t	Time
10. u	Fluid Velocity Vector
11. U	Characteristic Fluid Velocity
12. α	Inertial Resistance Coefficient
13. β	Viscous Resistance Coefficient
14. ∂	Partial Derivative Operator
15. δ	Characteristic Pore Length
16. ∇	Gradient Operator
17. ψ	Piezometric Head
18. ρ	Fluid Density
19. μ	Fluid Viscosity

1. Introduction

Sustainability has become a buzzword signifying change. As fossil fuel reserves dwindle the incentive to develop innovative technologies that are cost-competitive with the status quo has increased dramatically. These technologies address a desire to move away from wasteful practices and embrace less carbon intensive alternatives without sacrificing performance and dependability. Examples abound in modern society, as windmill farms and solar arrays spring up almost overnight, vehicle efficiency is increasing to combat rising fuel prices, and advanced sequestration techniques are implemented to reduce power plant emissions. Fossil fuel usage is not limited to the energy sector; industry accounted for approximately 27% of CO_2 emissions in the United States in 2012, including indirect emissions associated with electricity consumption [1]. The industry sector used approximately one third of all energy generated for the same year [2]. Manufacturing accounts for 80% of the industry sector in the United States [3]. Given the large energy consumption seen in the manufacturing industry, implementation of sustainable practices and development of products utilizing renewable materials is a logical way to reduce emissions and energy consumption.

In the eyes of businessmen, sustainability is also a hot-button issue whose implementation is crucial to being competitive in today's market. Managers of companies worldwide are committing to sustainability; 70% of managers responding to an MIT Sloan survey permanently have sustainability on their agendas [4]. This is especially surprising given that the economy is still recovering from the recession and indicates a growing trend. Resource-intensive industries ranging from energy and utilities to automobiles are leading the way [4]. Data also show that a company will make the shift

towards sustainability for the consumer [4]. The drive for sustainable practices is coming from the top and the bottom of the manufacturing industry.

What was somewhat of a niche role in the manufacturing industry many years ago is now commonplace. Some manufacturers focus their efforts on implementing sustainable practices while newer companies are founded on the premise of sustainability. Sustainability, at the time of its ideological conception, was defined to be "[practices] that meet the needs of the present without compromising the ability of future generations to meet their own needs" [5]. The definition is no longer limited to conserving energy and reducing the carbon footprint. It has evolved to encompass societal, environmental, and economical aspects [5].

Manufacturing enterprises are being founded to address their own interpretation of sustainability. As discussed earlier, the volume of CO_2 emissions that can be attributed to the manufacturing industry is significant. Reductions can come in the traditional sense, such as an increase in energy efficiency leading to a decrease in a company's carbon footprint. The manufactured product itself presents a different opportunity to incorporate sustainability into the industry. Plastics and polymers are an easy example of products derived from petroleum. Products made with these materials often end up in landfills; a large percentage of recyclable plastics do as well. Replacing plastic with a less carbon-intensive alternative is an avenue for sustainability recently being explored.

Ecovative is company that manufactures products out of a mushroom-based biodegradable compound [6]. These mushroom materials have been successful in a market saturated with competitors using age-old technologies, generating headlines mixed with equal parts praise and incredulity. "Can mushrooms replace plastic?"

headlined The Guardian [6]; “Form and Fungus” was the title of a New Yorker article [7]. Ecovative engineered a compound that combines recycled agricultural waste with mycelia, a root-like portion of a fungus, to create a product that is a good alternative to the traditional petroleum-based plastic [6, 8]. Applications range from surfboards and car parts to a substitute for Styrofoam [9]. Their success as a green manufacturer and knowledge of the technical specifications of their product has been pronounced, and inspired an investigation of further structural applications of the mycelia-based composite.

The core of a sandwich structure is a logical application for the mycelia composite due to its light weight. Sandwich structures are composed of thin, stiff sheets separated by a lightweight core bound together with adhesive [10]. The sheets contribute strength to an otherwise fragile core; the structure’s moment of inertia increases with a negligible increase in its overall mass, resulting in increased bending stiffness and bending strength [10]. The structure’s sheets can be made with a combination of polymerized natural oils and natural fibers, resulting in a composite that is a sustainable alternative to the petroleum-based sandwich structures.

The problem now comes down to efficiently manufacturing sheets for the sandwich structure. Two methods are being considered. The sheets could be produced independently and then adhered to the mycelia core, while another option involves stiffening an outer layer of the mycelia core. Both methods could be completed via vacuum infusion, a process depicted in Figure 1 [11]. Vacuum infusion is a process in which a pressure differential is used to induce resin flow through a material [11]. For the second method of creating the sandwich structure, it is important to maintain the

lightweight aspect of the core; a resin penetration of approximately 1/16 to 1/8 inches into the core is desired.

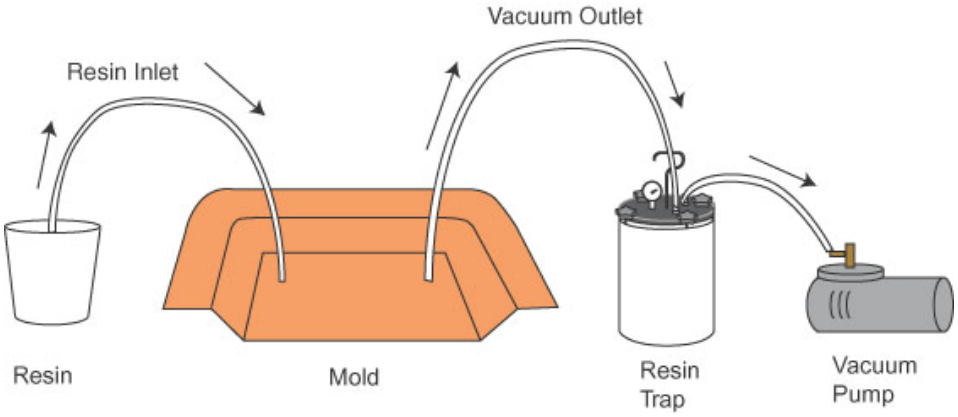

Fig. 1: Simplified depiction of vacuum infusion process [11].

While vacuum infusion is an efficient means of making composites with a good fiber to resin ratio, developing a quality product is largely an exercise in trial and error [11]. It is therefore prudent to conceptualize the problem on a small scale before attempting to coat larger parts in resin. An understanding of vacuum infusion will also allow for efficient manufacturing of the sandwich structure, keeping true to the sustainable nature of the mycelia product itself.

This project addressed the challenges of resin infusion. Computational Fluid Dynamics (CFD) models of vacuum-induced resin infusion were developed in Star CCM+, a commercial CFD software package. Research to investigate using carbon fiber mats as the base material for the sheet layers of the sandwich structure is being conducted. A mold that integrated features theoretically conducive to enhanced resin dispersion around the mycelia core is investigated. Plenums, vacant area before and after the carbon fiber mat, are included in the mold; resin is expected to fill the plenum before

flowing through the carbon mat. A more uniform resin flow through the carbon mat is anticipated with the addition of plenums to the mold.

The mycelia core and carbon fiber mats were modeled with porous interfaces and regions within Star CCM+. This stage of modeling focused on the flow of resin between the sandwich layers and the mycelia core, with the objective of minimizing fluid flow through the core. Optimization of the resin infusion will result in a product with enhanced stiffness and durability while maintaining a lightweight mycelia core.

This paper provides documentation for the modeling process described. An overview of developing models in Star CCM+ and the fluid mechanics governing fluid flow through porous media within the software is presented. Modeling considerations specific to vacuum infusion are discussed. Treatment of porous media in Star CCM+ and experimental treatment of similar media is compared. Finally, modeling methodology is presented, followed by a discussion of simulation results and plans for future work.

2. Background

Fluid flow in porous media has been thoroughly studied and is present in many industrial and manufacturing applications. Perhaps the most notable field of application is fluid flow beneath the surface of the earth. Flow of ground water and oil are some examples [13]. Although such flow involves complex configurations of cracks that fluid passes through, discretizing porous media into open and closed areas provides a good foundation for understanding the flow on a conceptual basis.

Darcy's Law is a relationship that relates volumetric flow driven by a pressure differential and the properties of the porous media [12]. Darcy's Law for groundwater flow is illustrated in Figure 2 [13]. Although the Darcy's Law was derived experimentally for groundwater flow, its viability for approximating flow through porous media has been demonstrated [12]. Flow is approximated by calculating flow as if it's uninhibited and applying a correction factor. Part of this factor is permeability, a material property that quantifies the resistance to fluid flow within a material [12]. The dynamic viscosity of the fluid also plays a role [13].

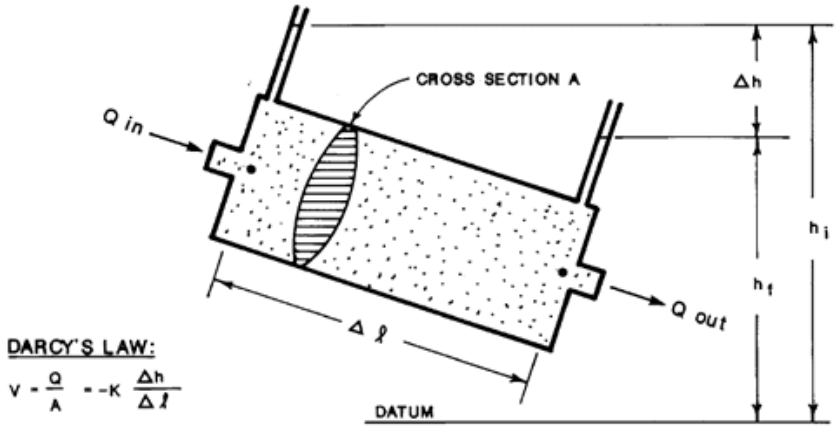

Figure 2: Schematic of Darcy's Law for groundwater flow [14].

CFD software computations utilize Darcy's Law in simulations involving porous media. The fluid mechanics governing flow in porous media will be presented in this section, followed by a description of vacuum infusion modeling. An overview of the Star CCM+ workflow and a detailed account of treatment of porous media in the simulation software will conclude the section.

2.1. Fluid Flow in Porous Media

Two equations lie at the core of fluid mechanics: the conservation of mass and conservation of momentum, shown by Equation 1 and 2 [14]. The conservation of mass is straightforward; it mathematically states that the same mass of fluid entering a volume must be leaving the volume for a given time [14]. The conservation of momentum, also known as the Navier-Stokes equations, relates a fluid's change in momentum to forces acting on the fluid where u is the velocity vector, and p is pressure, f is a body force, and t is time [14]. Present in the equation are constants that characterize the fluid: density, ρ, and viscosity, μ. The equation also contains the gradient operator, ∇.

$$\nabla \cdot u = 0 \tag{1}$$

$$\rho(\frac{\partial u}{\partial t} + (u \cdot \nabla u)) - \mu \nabla^2 u + \nabla p = f \tag{2}$$

Equation 2 can be simplified to describe flow traveling through porous media [14, 15]. A coefficient characterizing this flow can be calculated as a ratio of the inertial and viscous forces, the Reynolds number, given by Equation 3a [14]. Terms U and L in Equation 3a are velocity and length values characteristic of the flow at length L [14]. The Reynolds number for flow within pores can be calculated with Equation 3b where δ is the characteristic pore length [14].

$$Re = \frac{\rho U L}{\mu} \quad (3a)$$

$$Re = \frac{\rho U \delta}{\mu} \quad (3b)$$

For low Reynolds number flows (Re << 1) viscous forces dominate and inertial terms in the Navier-Stokes equation can be ignored [14, 15]. The modified form of Equation 2 for steady flow is Equation 4 [14, 15]. In cases where body forces such as gravity can be ignored, Equation 4 can be simplified further into Equation 5.

$$-\mu \nabla^2 u + \nabla p = f \quad (4)$$

$$\nabla p = \mu \nabla^2 u \quad (5)$$

Equation 5 must be modified to be accurate on a macroscopic scale to adequately represent flow through porous media; it currently only describes fluid flow in individual pores [14, 15]. This can be done with Darcy's Law, shown in Equation 6 [14].

$$q = \left(\frac{-k}{\mu}\right) \cdot \nabla \psi \quad (6)$$

Darcy's Law relates pressure and volumetric fluid flow rate through a porous solid, neglecting inertial effects and assuming incompressible flow [14]. The flow flux, q, is related to the permeability tensor, k, the piezometric head, ψ, and the fluid viscosity [14]. For applications neglecting gravity, ψ is equivalent to the gradient of pressure [14]. As described earlier, permeability quantifies the level of resistance to flow within porous media. Rearranging Equation 6 in terms of the pressure gradient yields Equation 7a [14]. For flow in one coordinate direction, the gradient operator can be removed via integration [14]. Values on the diagonal of the permeability tensor are equivalent for isotropic materials [14]. Applying these simplifications resolves Equation 7a into Equation 8a [14]. For further simplicity, Equation 7a and 8a are rewritten in terms of fluid velocity,

yielding Equations 7b and 8b. The flux, q, is a function of porosity [16, 17]. Porosity is lumped in with density for unsteady simulations in Star CCM+, allowing the flux to be replaced with velocity [16, 17].

$$\nabla p = \frac{-q\mu}{k} \tag{7a}$$

$$\nabla p = \frac{-u\mu}{k} \tag{7b}$$

$$\Delta p = \frac{-q_i \mu \Delta L_i}{k_{ii}} \tag{8a}$$

$$\Delta p = \frac{-u_i \mu \Delta L_i}{k_{ii}} \tag{8b}$$

Fluid properties and material properties must be known to make use of the equations detailed in this section. Equation 8b can be used to calculate permeability using experimental data. Analytical methods can also be used to estimate permeability from other physical properties of porous media. For this project, it is assumed that the permeability of the modeled porous media is known.

2.2. Modeling Vacuum Infusion

The properties of a porous medium can change when it is subjected to a large pressure differential. Models must accurately account for conditions induced by the vacuum to make simulation efforts worthwhile. Due to the increase in production and widespread usage of composite materials, efforts have been made to develop numerical models for the resin infusion of composites.

Computational simulation programs such as PAM-RTM are available to model resin infusion in an industrial setting [18]. Such software has the capability to predict time to fill a mold with resin and the location of the leading edge of resin (flow front)

within the mold [18]. Efforts to increase the fidelity of these programs to address minutia introduced by vacuum molding have been conducted [18, 19].

As introduced earlier, vacuum infusion drives resin flow via a negative pressure differential. A core preform is placed within a vacuum bag and is subsequently subjected to the pressure differential and resin flow [18]. Due to the application of a vacuum, the preform is subjected to compression [18]. The compression therefore impacts the permeability of the preform core [18]. Changes in the viscosity of the material can also result for non-newtonian resins [18]. For scenarios where incompressible and Newtonian fluid assumptions are reasonable, Darcy's Law models resin flow fairly well [18].

A key difference between the theoretical and realistic applications of Darcy's Law exists at the edges of the preform where there is less resistance to fluid flow [19]. This has been observed experimentally and can be adequately accounted for in simulations by increasing the permeability of a porous region near its edges [19]. Increasing the permeability near the edge of a porous region by a factor of one hundred allows simulated and experimental results to agree [19].

2.3. Star CCM+

Star CCM+ simulations are a product of a number of steps. Before a simulation can be conducted, geometry must be created in a Computer Aided Design (CAD) program, physics and geometric discretization models must be selected, and a solving regions need to be generation. Results can be analyzed after convergence of the simulation in Star CCM+ itself or exported for manipulation within other data analysis software.

Counterintuitively, models in Star CCM+ work with negative space. For example, empty space within a mold must be imported as a solid for modeling fluid flow within the mold. Star CCM+ supports various Computer Aided Design (CAD) files and has built in CAD capabilities for further manipulation if necessary. Contained within the software are the abilities to manipulate geometry spatially (e.g. translation, scaling) and perform Boolean operations to create new parts. The geometry, once finished, can then be broken down into sections. These sections are used to define regions: various types of inlets and outlets, walls, and symmetry planes. Boundary and surface conditions are defined by the user for each region.

The regions are then discretized through a process called meshing. Meshing models are included in Star CCM+ that divides input geometry into individual solving volumes. Models can be selected to create cells of different shapes and sizes depending on the goals of the simulation and preference of the user. A generic, robust meshing model discretizes the geometry into polygons, whereas other meshing models create rectangles or triangles. The user specifies a base cell size based on model geometry; models with high resolution have a high cell count and take much longer to converge than those with lower resolution. Models with high fidelity generally lead to more accurate solutions, however.

Physics models governing fluid flow are then selected based on the modeler's understanding of fluid mechanics governing the fluid flow. Fluid phase, flow and turbulence models, and continuum models can be selected as necessary. Various turbulence models are contained within the software.

Conducting simulations for complex geometries is computationally expensive. This presents a problem when modeling porous media because explicitly modeling the open and closed regions within a porous solid quickly becomes infeasible for large solids. Fortunately, there are methods for dealing with porous media that are good alternatives, offering insight into flow through the porous region on a macroscopic scale and the effect of the solid on flow externally.

2.3.1. Porous Media in Star CCM+

There are two methods of modeling porous media in Star CCM+. Porous baffle interfaces, traditionally used to model perforated plates and wire screens, can be used to model porous media in Star CCM+ [20]. A second option is defining an entire region as a porous medium [22]. Both methods can be used to determine the macroscopic effect isotropic porous media will have on the flow, but are implemented differently within the software [16, 18]. Fluid passing into the porous medium will be subjected to a pressure gradient that simulates resistance it would otherwise encounter within the medium, calculated from parameters input by the user [20, 22]. The porosity and viscous and inertial resistance of the porous media must be specified [20, 22]. Treatment of porous baffle interfaces will be discussed briefly, followed by an analogous discussion of treatment of porous regions within the software.

Star CCM+ uses Equation 9 to calculate the pressure differential across a porous baffle interface [20]. Coefficients α and β correspond to the inertial and viscous resistance, respectively, of the porous medium [20]. The expected flow will be highly viscous and laminar. Constant β will therefore be the only factor in the pressure differential, as shown in Equation 10.

$$\Delta p = -\rho(\alpha|u| + \beta)u \quad (9)$$

$$\Delta p = -\rho\beta u \quad (10)$$

Coefficients α and β are usually determined empirically by fitting power curves to experimental velocity and pressure data [21]. An alternate method to calculate the coefficients exists. Equation 10 has roots in the Navier-Stokes equation and bears a direct resemblance to Darcy's Law. Comparing the two will yield a method to estimate β. This comparison is shown in Equation 11. Equation 12 can therefore be used to calculate β.

$$\Delta p = -\rho\beta u = \frac{-u\mu\Delta L}{k} \quad (11)$$

$$\beta = \frac{\mu\Delta L}{\rho k} \quad (12)$$

Modeling porous media as a full region is more straightforward. The resistance of a porous region to flow is calculated with Equation 13 in Star CCM+ [22]. The right-hand side of Equation 13 is composed of P_v and P_i, the medium's viscous and inertial resistance coefficients. Neglecting inertial effects again, the pressure drop analogous to that seen in Equation 10 is expressed in Equation 14 [22]. Equation 15 can be used to calculate the viscous resistance components for application to porous regions in Star CCM+ [17]. Comparing Equations 14 and 15, it is easy to obtain a relationship for P_v, shown as Equation 16. Given that Equations 13 through 16 are equivalent to Equations 7 and 8, modeling porous media as porous regions in Star CCM+ will be the preferred method.

$$\frac{\Delta P}{\Delta L} = -(P_v + P_i|u|)u \quad (13)$$

$$\frac{\Delta P}{\Delta L} = -P_v u \quad (14)$$

$$\nabla P = \frac{-u\mu}{k} \quad (15)$$

$$P_v = \frac{-\mu}{k} \quad (16)$$

The fluid mechanics governing treatment of porous media have been detailed. Darcy's Law is used to quantify the resistance to flow of porous media. Problems can arise during simulation that must be solved through experimental analysis. For example, the permeability of a porous medium must be known to accurately model it in CFD software. Even once a problem has been tackled numerically, simulations should be validated with experimental results.

2.4. Experimental Treatment of Porous Media

Various experimental works have been conducted to understand flow through complex porous media. Whereas the macroscopic effect is considered in CFD computations outlined earlier, the microscopic effect can only be analyzed numerically by modeling the geometry explicitly. In scenarios where it is prudent to understand fluid flow on the micro-scale, experimental methods of monitoring exist. Flow can often be characterized via magnetic resonance imaging and x-ray techniques [12, 14]. These methods are robust but do not allow for quick imaging [12]. When sufficient computational resources are available, small-scale CFD simulations can be conducted with explicitly modeled pores. Imaging techniques described can be used to generate CAD files for import into CFD software. Given that the scope of this project is macroscopic, concerning the overall impact of the mycelia core on resin flow, numerical techniques will provide insight to the level of detail desired. The next sections describe modeling methodology and discuss simulation results. Modeling methodology

incorporates features in Star CCM+ described earlier and takes steps to address for challenges introduced by vacuum infusion.

3. Methodology

Creating stiff sheets and a lightweight core separately and then bonding the components together post-production is a logical way to manufacture sandwich structures. Ecovative's mycelia-based material is a logical candidate for the core, but research and experimentation is needed to identify materials suitable for usage in the stiff sheets. Carbon fiber sheets, a lightweight and strong fabric are one possibility being examined. Experimental work to investigate the viability of carbon fiber for this application is being conducted in tandem with the modeling described in this thesis. This section will document the methodology behind modeling such vacuum infusion in Star CCM+. An overview of the experimental setup and a description of the experimental mold will be given. An account of the transition between the experiment and the simulation will then be provided, followed by detailed documentation of the procedure used to create the simulation in Star CCM+.

3.1. Transition from Experiment to Simulation

The experimental set up resembles vacuum infusion as depicted in Figure 1. A pressure differential induced by a vacuum will drive resin flow through carbon fiber sheets. A see-through mold contains the carbon fiber, allowing for observation of resin flow during the infusion process. The mold was rendered in SolidWorks; a front view of the mold showing the inlet and a cross section showing open space in the mold is contained in Figure 3.

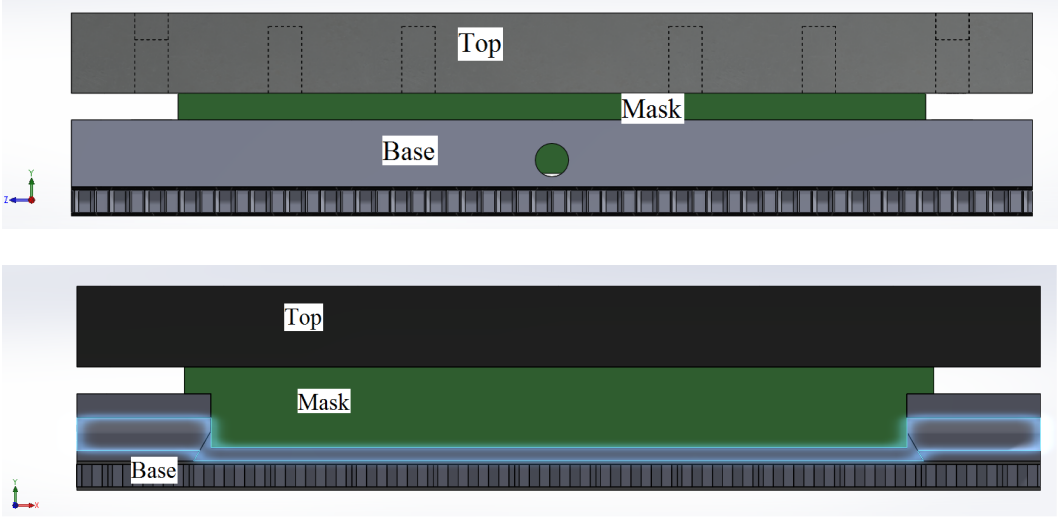

Fig. 3, Top: Front view. Bottom: Cross section of mold. In the top and bottom images the top and base sections of the mold are shown in grey. The mask is shown in green. The mold cavity is outlined in blue in the bottom image.

The mold consists of three major components: the base and top, shown in grey, and mask, shown in green. The gap between the mask and the mold in Figure 3 (bottom) measures approximately 6.5 by 6.5 by 1/8 inches. A mat of carbon fiber is inserted into the open region below the green mask for experimentation. The mask aids in obtaining a tight seal for the vacuum infusion process. As discussed earlier, Star CCM+ simulations require CAD input to be representative of negative space, or area that fluid can flow through. The empty area outlined in blue in Figure 3 (bottom) must be imported as a solid for modeling. This solid is shown in Figure 4 and was created in SolidWorks. Plenums are visible on the left and right sides of the open area adjacent to the inlet and outlet ports in Figure 4. The plenum closest to the mold inlet is annotated in Figure 4.

Fig. 4: CAD solid imported into Star CCM+ for modeling. This solid was created in SolidWorks and is analogous to the open area outlined in blue shown in Figure 3 (bottom). The mold inlet is visible on the left of the image; the outlet is visible on the right.

A 6K, 5HS variant of carbon fiber was used to create the mat for experimental testing [23]. The mat generally consisted of four to five layers of the carbon fiber. Its permeability was determined to be 3500 Darcy experimentally [23]. An extra sheet of carbon fiber was added to the mat during the permeability tests to simulate compression of the mat induced by the vacuum. The porosity of the carbon mat was also measured to be 0.63 [23, 24].

The infusion of the carbon mat with two resins, Resin A and Resin B, was of interest. The viscosity of Resin A was determined to be 1100 centipoises (cp) [23]. Resin B was measured to have a viscosity of 470cp [23]. The resins have a density roughly equivalent to that of corn syrup, 1406 $\frac{kg}{m^3}$ [24, 25].

3.2. Modeling in Star CCM+

This section will document the procedure used to generate, run, and extract data from the Star CCM+ simulations created for this project. Region discretization and selection of meshing models are presented first. An overview of physics models selection and incorporation of porous media follows. A description of running a model in Star CCM+ and extracting data from completed simulations concludes the section.

3.2.1. Region Initialization

Mold geometry was imported into Star CCM+ as a parasolid (".x_t" file extension). This method of transferring the geometry from SolidWorks to Star CCM+ facilitates further manipulation within the CFD software. Geometry shown in Figure 4 was divided into three sections, shown in Figure 5, to allow for application of porous media modeling techniques. Sections outlined in blue were modeled as porous regions whose physics was explained in Section 2.3.1. The outer porous section in Figure 5 is 1/16 inches thick on all sides, making the inner porous section a 6.375 by 6.375 inch square. The depth of both sections did not change. The remaining section containing the inlet and outlet ports remained a traditional fluid region.

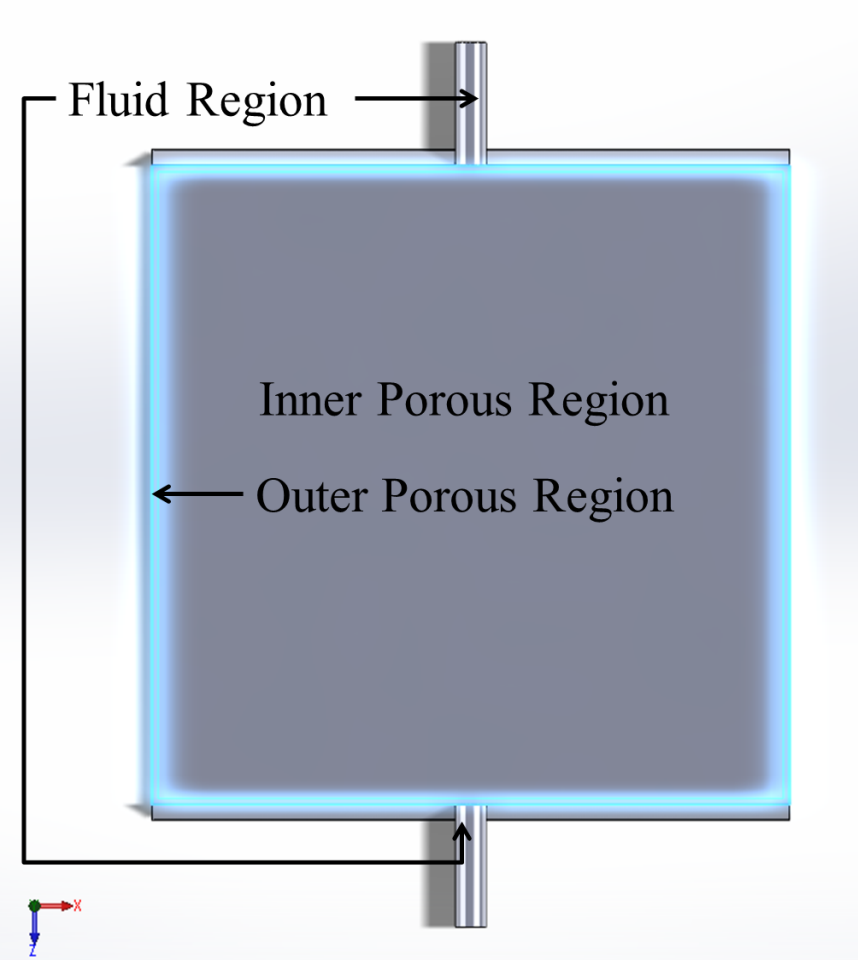

Fig. 5: Mold geometry divided into three sections: two porous regions and one fluid region.

Importing the geometry from a parasolid file format allowed for each section to enter the CFD software as a separate part. Three separate, non-intersecting sections were created by using a Boolean subtract operation, creating the highlighted sections shown in Figure 6.

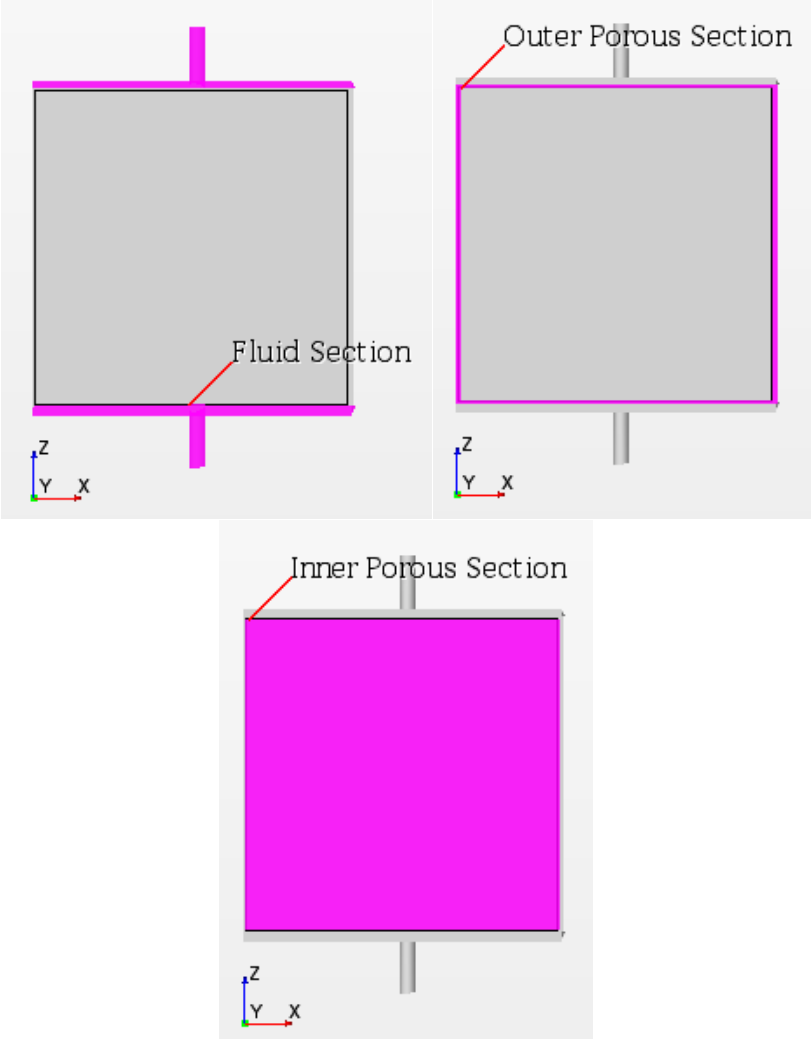

Fig. 6 Left: Fluid section. Center: Outer porous section. Right: Inner porous section.

Sections were then split into different surfaces using the “split by patch” tool in Star CCM+. This separation allows for designation of inlet and outlet ports for the fluid section and for the creation of interfaces between adjacent faces in the geometry. Interfaces are required to allow flow between parts. The fluid section was split into five surfaces, two of which will be used to create interfaces. Similarly, the inner and outer porous sections were split into multiple surfaces for the creation of interfaces to allow flow between them.

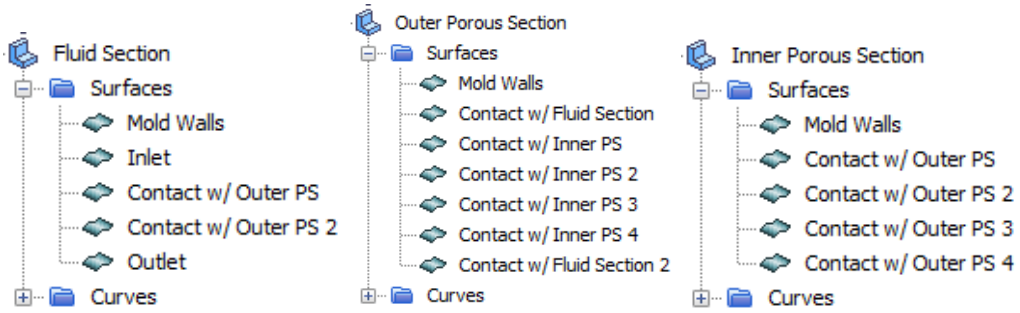

Fig. 7 Left: Surfaces in fluid section. Center: Surfaces in outer porous section. Right: Inner porous section surfaces. “Porous Section” has been abbreviated as PS.

The newly divided sections were assigned to regions in Star CCM+. Assigning the geometry shown in Figures 6 and 7 to regions allows each section to be discretized by meshing algorithms in Star CCM+. The sections modeled as porous media can also be configured after being designated as regions and boundary conditions can be applied to the inlet and outlet ports of the fluid region. Figure 8 illustrates how to assign parts to regions. It is important to note that options “Create a Region for Each Part” and “Create a Boundary for Each Part Surface” were selected. These options ensured that each section becomes its own region and that surfaces shown in Figure 7 remain separate for individual manipulation.

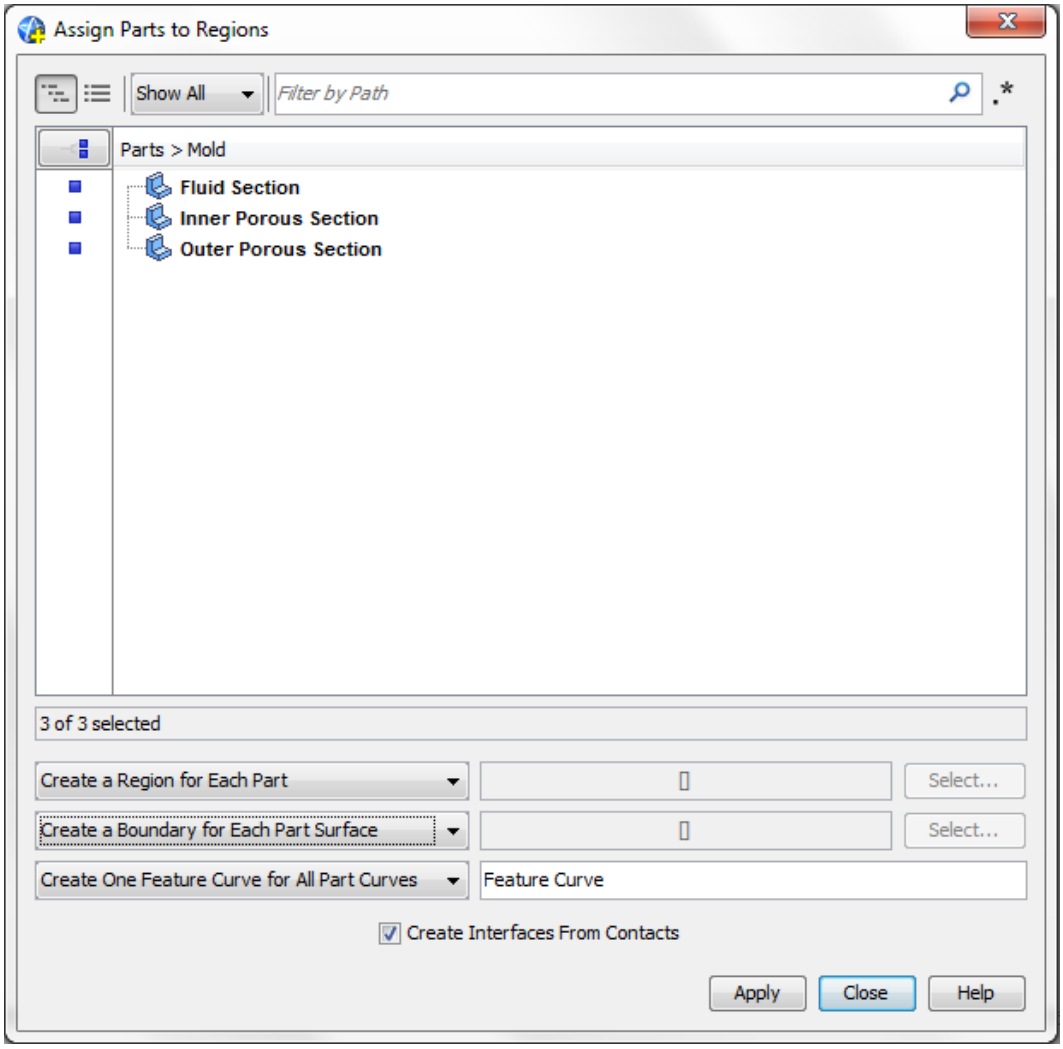

Fig. 8: Assigning parts to regions in Star CCM+. "Create a Region for Each Part" and "Create a Boundary for Each Part Surface" options were selected.

Three regions were created: a fluid region, and two regions to be modeled as porous media. The default region assignment in Star CCM+ is a fluid region. The inner and outer porous sections were changed from fluid regions to porous regions, shown in Figure 9.

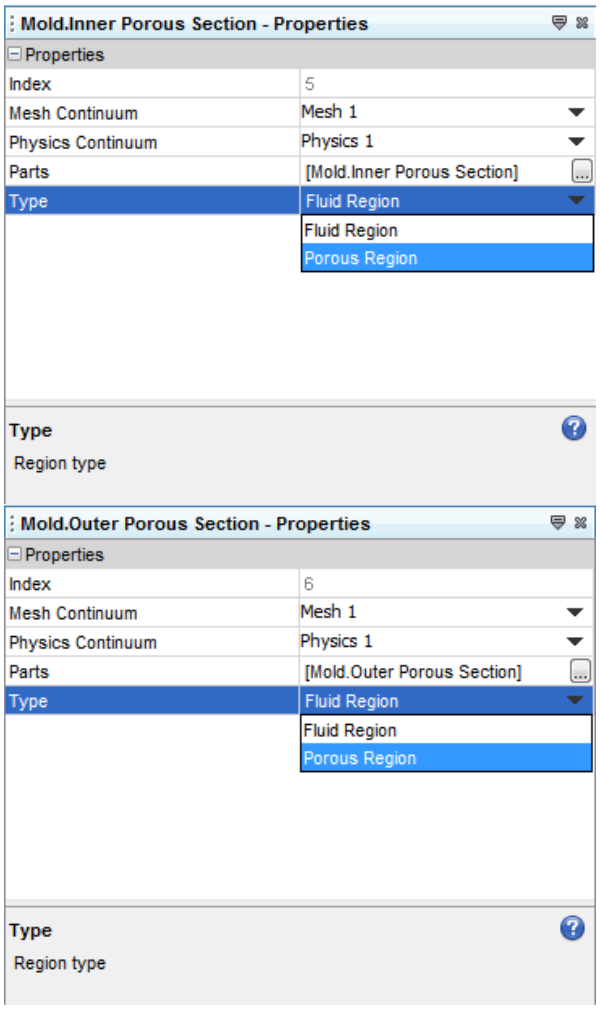

Fig. 9: Changing porous sections from fluid to porous regions in Star CCM+. A region's properties menu can be accessed by selecting the region in the menu on the left side of the screen in Star CCM+.

3.2.2. Meshing Model Regions

As described in Section 2.3, meshing models available in Star CCM+ are used to discretize a volumetric region into small subsections called cells. Continuum and conservation equations are iteratively solved within each cell to compute a solution.

There are two steps in generating meshes for simulations. The first is creating surface mesh, a process in which the regions are enveloped in a triangle-based mesh.

Generating a surface mesh aids the second step of meshing: generating a volume mesh. The volume meshing stage divides regions into the cells.

For models created for this thesis, the "Surface Remesher" model was always used for creating a surface mesh. There were two model options for generating a volume mesh. "Trimmer" and "Prism Layer Mesher" models were selected over using the "Advancing Layer Mesher." The key difference between Trimmer and Advancing Layer Mesher meshing models is their discretization shape. The Advancing Layer Mesher is the most efficient way of discretizing regions in Star CCM+, in that it results in models that run slightly faster. The Advancing Layer Mesher discretizes regions into polyhedral cells, whereas the Trimmer generates a volume mesh out of square cells. To preserve the ability to easily monitor the number of cells filled with resin, the Trimmer was selected for simplicity. The Trimmer model was coupled with the Prism Layer Mesher to ensure that small cells were generated near the walls in the fluid and porous regions. Selection of meshing models is shown in Figures 10 and 11. A different mesh continuum is needed for each region, making three necessary. A new continuum can be created by right clicking the continua folder in the menu on the left side of the screen in Star CCM+. Figure 10 demonstrates how to create a new mesh continuum; Figure 11 shows the selection of meshing models.

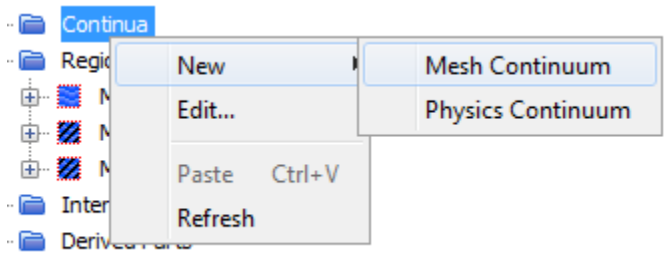

Fig. 10: Creating a new mesh continuum. A new continuum can be created by right clicking the continua folder in the menu on the left side of the screen in Star CCM+.

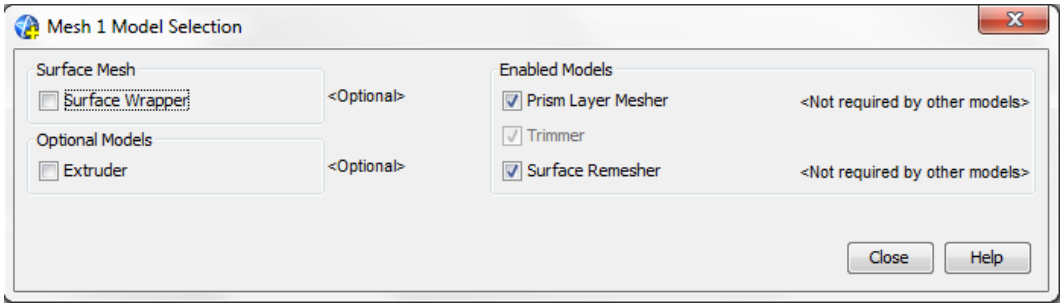

Fig. 11: Selection of mesh models. Meshing models can be selected by opening a newly created mesh continuum's dropdown menu and double clicking on the "models" folder.

Meshes were configured once the meshing models were selected. The base size of each mesh was set to be 0.0075 meters. Each mesh was modified further to include five prism layers, set to be five percent of the base size with a prism layer stretching coefficient of 1.3. The regions were subsequently meshed, ending with a total of 116224 cells. Figure 12 shows how to retrieve these values from a mesh continuum's dropdown menu. An image of the final mesh is contained in Figure 13.

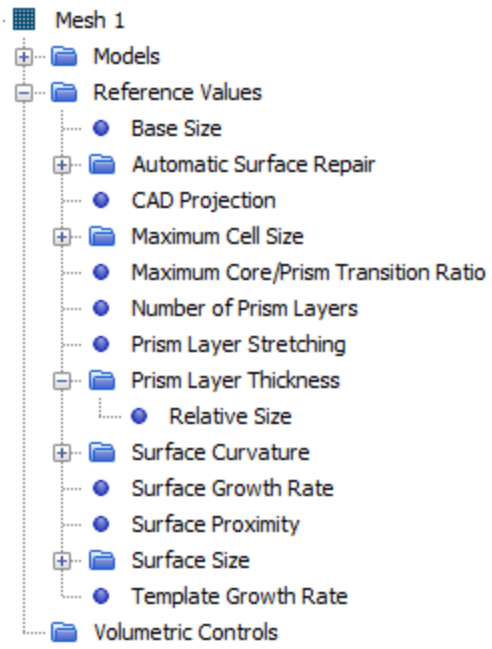

Fig. 12: Image of a mesh continuum's dropdown menu. Within this menu base size, prism layer, stretching, and layer relative size values for the mesh can be accessed for modification.

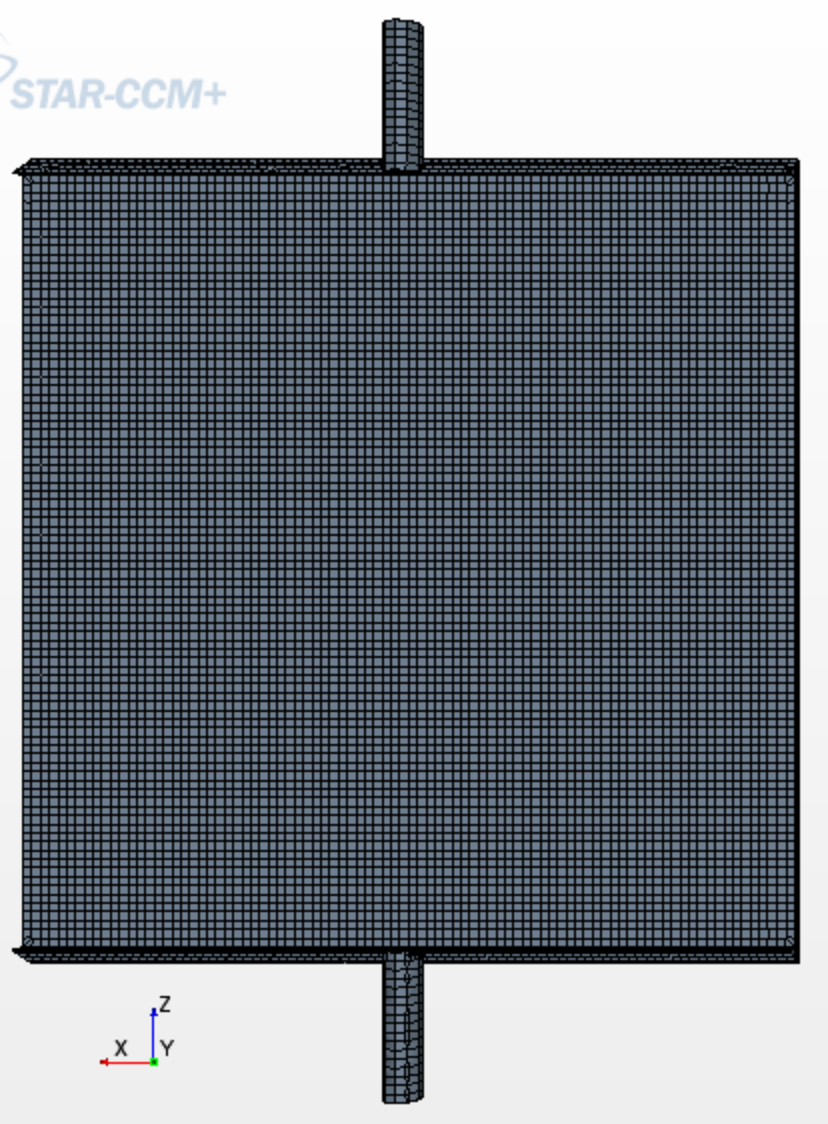

Fig. 13: Image of completed mesh.

3.2.3. Selection of Physics Models

Section 2.2 presented a few assumptions implicit in modeling porous media with Darcy's Law. The first assumption is that the fluid is incompressible. Secondly, the modeled fluid must be Newtonian. These assumptions hold for Resins A and B [24]. The applicable physics models were chosen after a new physics continuum was created. This was done in the same way new mesh continuum was created, shown in Figure 11.

Figure 14 illustrates the selected models. In addition to the incompressible assumption, flow was assumed to be Laminar due to the low expected fluid velocities. An unsteady model was chosen to incorporate the physical passage of time. Default models "Gradients" and "Three Dimensional" were automatically included by the CFD software.

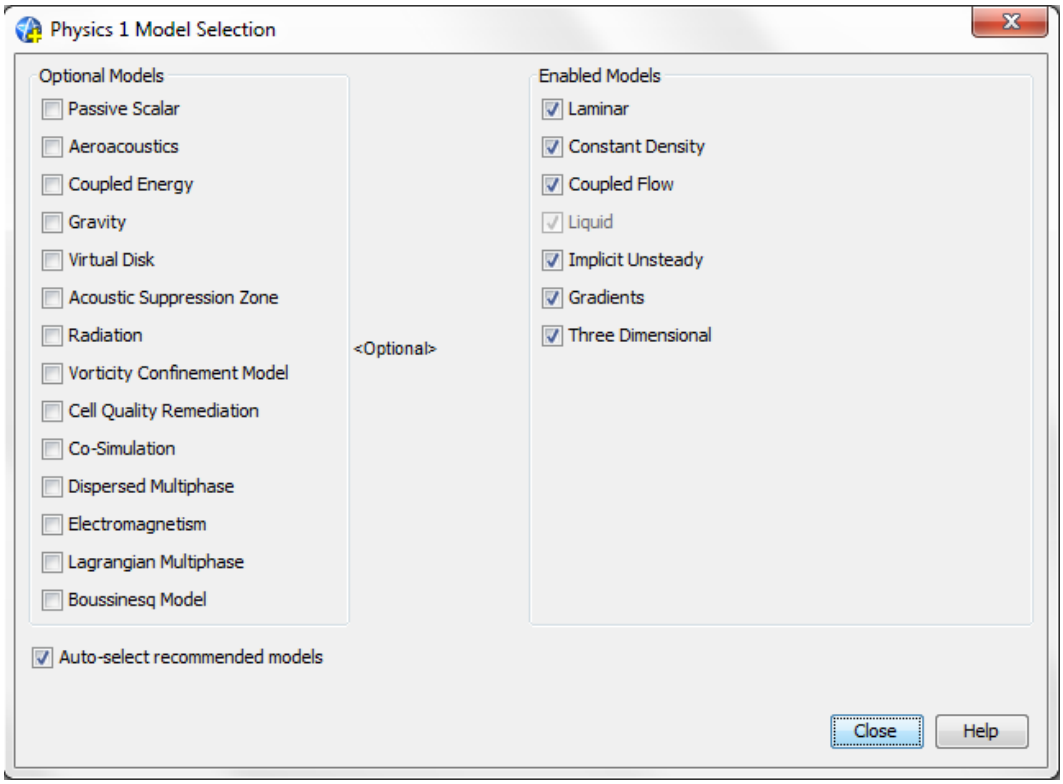

Fig. 14: Selection of physics models. Physics models can be selected after creating a physics continuum. Then the menu shown can be accessed by double clicking the "models" folder accessible after the physics continuum's dropdown menu is opened.

The default values in the physics models were then adjusted. Dynamic viscosity and density values for Resin A were entered. Values were changed for simulations involving Resin B. Figure 15 shows how to find viscosity and density, accessed by expanding the physics continuum dropdown menu.

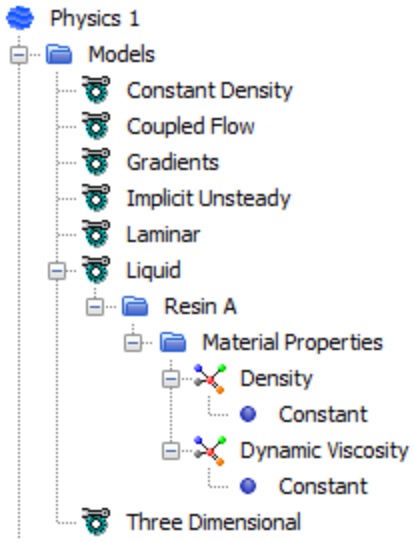

Fig. 15: Image of a physics continuum's dropdown menu. Within this menu dynamic viscosity and density values can be accessed for modification.

3.2.4. Region Finalization

The porous regions were then configured. Material properties of each porous region were then configured. Using Equation 16 the viscous resistance of the region can be calculated. The carbon fiber mat was assumed to be isotropic, allowing both porous regions to be modeled with a constant viscous resistance. Strategies discussed in Section 2.2 to address some challenges of modeling vacuum infusion were incorporated. The permeability of the outer porous region was modified to be one hundred times greater than the permeability of the inner porous region. The permeability of the carbon mat was also measured under simulated vacuum conditions. The Porosity of each region was also entered at this time and was assumed to be constant between regions. Because Equation 16 also depends on the viscosity of the fluid, different viscous resistances were used for simulations involving Resin A and those involving Resin B. Entered values are displayed in Table 1; resistance values were calculated using Equation 16.

Table 1: Viscous resistance and porosity values entered for both porous regions for each Resin. Porosity is unit less. Viscous resistance is listed in units of $\frac{kg}{m^3 \times s}$.

	Inner Region		Outer Region	
	Porosity	Viscous Resistance	Porosity	Viscous Resistance
Resin A	0.63	318450000	0.63	3184500
Resin B	0.63	136060000	0.63	1360600

Figure 16 illustrates how to retrieve these values for the outer porous region, accessed by opening the "Physics Values" dropdown menu within the region's own dropdown menu.

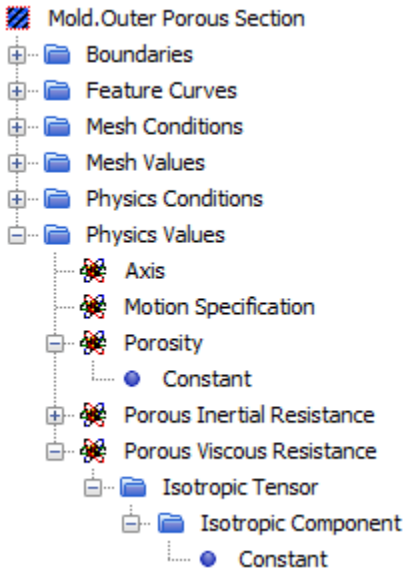

Fig. 16: Image of a porous region's dropdown menu. This menu can be found by first expanding the general regions dropdown menu and then expanding a specific region's menu, both found on the left side of the Star CCM+ window. Within this menu porosity and viscous resistance constants can be accessed for modification.

Interfaces to allow fluid flow between regions were then created. Two interfaces from the fluid region to the outer porous region were necessary to permit flow from the inlet tube to the porous regions, and again from the bottom of the porous regions to the

outlet tube. Interfaces between the outer and inner porous regions were also created. Figure 17 illustrates how to create an interface in Star CCM+. Creating an interface is an option that appears after right-clicking the associated section boundaries. Figure 18 shows the interfaces created for each region.

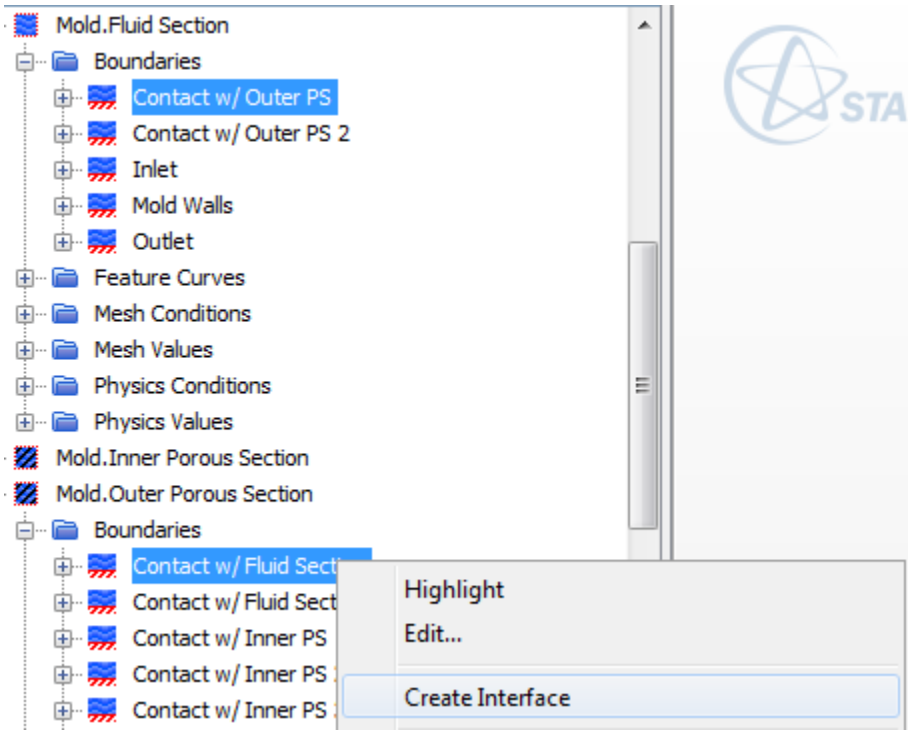

Fig. 17: Image of creating an interface in Star CCM+. Interfaces can be created by selecting both of the desired regions and then right clicking and selecting “Create Interface” as shown.

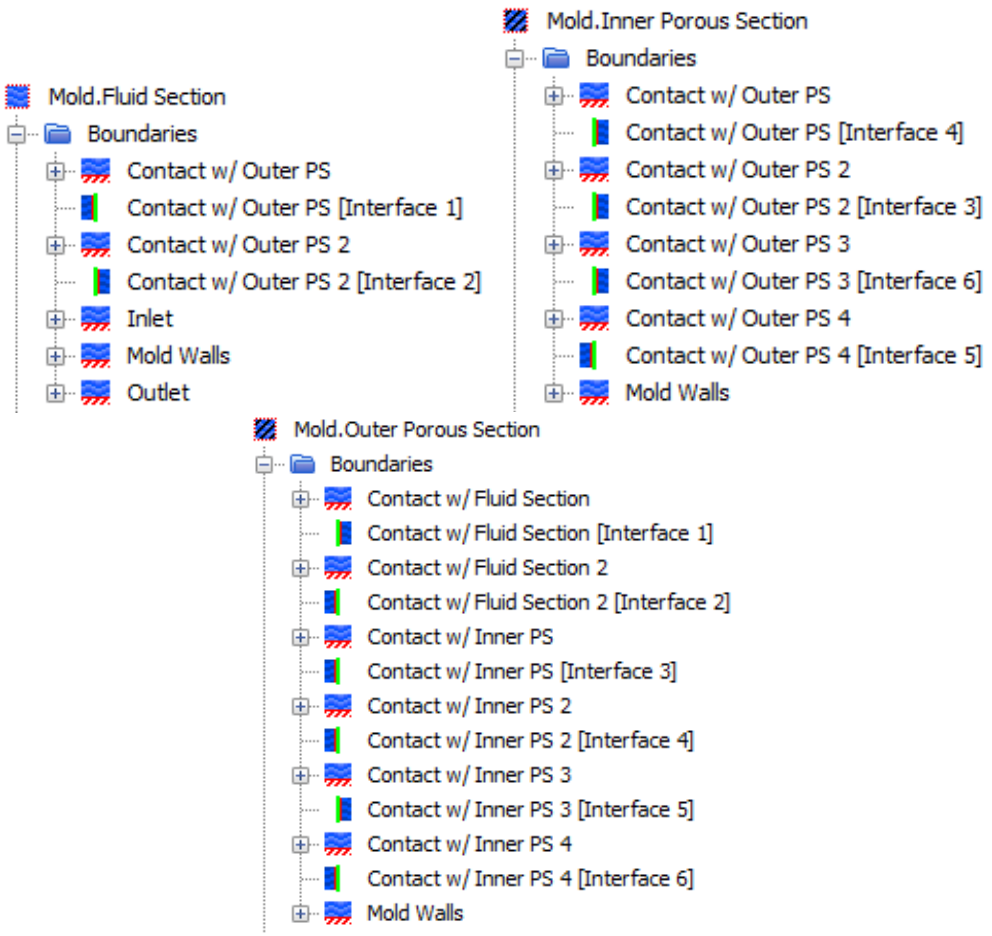

Fig. 18: Interfaces created for each region. Interfaces are represented by half-squares with vertical green lines below a section boundary.

The last step in configuring the regions is defining faces in the fluid region as inlet and outlet ports, respectively. For modeling fluid flow driven by a pressure differential, the inlet is defined as a stagnation inlet in Star CCM+ and the outlet is defined as a pressure outlet. The pressure at the inlet and outlet can be configured to replicate the differential induced by the vacuum. The default reference pressure is atmospheric pressure, 101325 Pascals (Pa). To model a vacuum-induce pressure differential the pressure at the outlet was set to -101325 Pa. Figure 19 shows how to change two fluid region boundaries to a stagnation inlet and a pressure outlet. Changing the pressure at the outlet is shown in Figure 20.

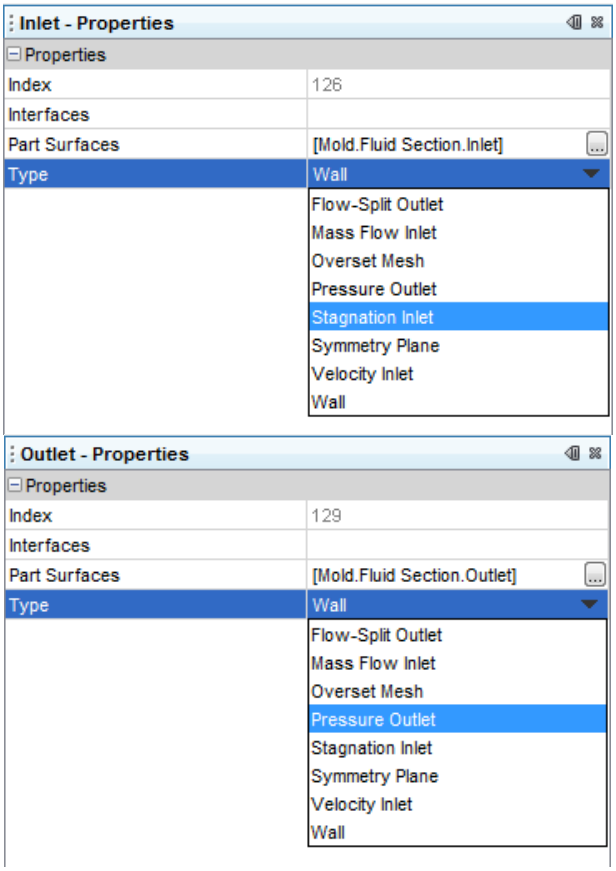

Fig. 19 Left: Making a boundary a stagnation inlet. Right: Making a boundary a pressure outlet. This menu can be accessed by expanding the fluid region on the left side of the Star CCM+ window so the region's boundaries can be seen. Then, the boundary can be changed from wall to inlet or outlet, respectively.

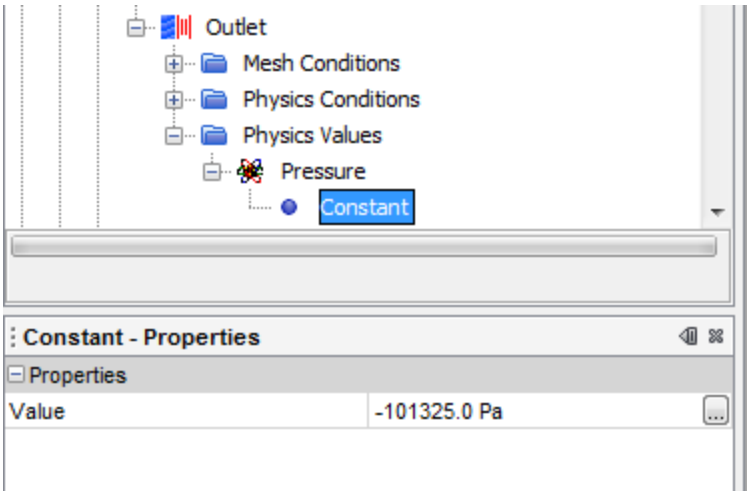

Fig. 20: Changing pressure at outlet of fluid region. This menu can be accessed by expanding the fluid region on the left side of the Star CCM+ window so the region's boundaries can be seen. Then, the "Outlet" boundary can be expanded to match the image seen above.

The mold geometry was imported into Star CCM+ and sections were divided into surfaces for the creation of interfaces. Sections to be modeled as porous media were modified to include known properties of the carbon fiber mat. The porous regions then accurately modeled the carbon fiber mat and incorporated practices common to modeling vacuum infusion. Physics models were also selected in accordance with assumptions necessary to model porous media with Darcy's Law.

3.2.5. Running a Simulation

Once geometry has been assigned to regions, meshed, and configured appropriately for the intended simulation, the simulation can be run. There are many ways to monitor a running simulation, the easiest of which happens automatically. A running simulation will plot "residuals," which are a numerical method of quantifying error between iterations in a simulation. The easiest way to know a simulation is "done" is to inspect the residual plot and ensure that they are not changing between iterations.

The number of iterations needed to arrive at a solution depends largely on the complexity of the simulation and its resolution; simulations with a large number of cells take longer to run.

Unsteady simulations can be automatically stopped in a number of ways. If the modeler has a good idea of how many iterations are necessary to obtain a solution, a maximum number of iterations can be enforced. Alternatively, a physical time limit can be set in place. Figure 21 shows where to find the stopping criteria in Star CCM+. "Inner Iterations" refer to the number of iterations done within each time step; the default time step is 0.001 seconds. The simulation will continue running until the "Maximum Steps" criterion is satisfied, meaning that the specified number of time steps has elapsed.

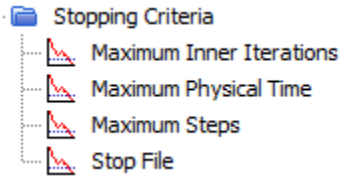

Fig. 21: Stopping criteria menu in Star CCM+. This menu can be found by expanding the "Stopping Criteria" folder on the left-hand toolbar in the Star CCM+ window.

In addition to monitoring the model residuals for consistency, other physical parameters should be observed for consistency with expected results. An easy parameter used to ascertain whether the simulation was running appropriately was fluid velocity; a model showing unnaturally high velocities would be investigated to ensure correct setup. Physical parameters for a running simulation can be visually monitored with a scalar or vector scene, created by right-clicking the "Scenes" menu shown in Figure 22.

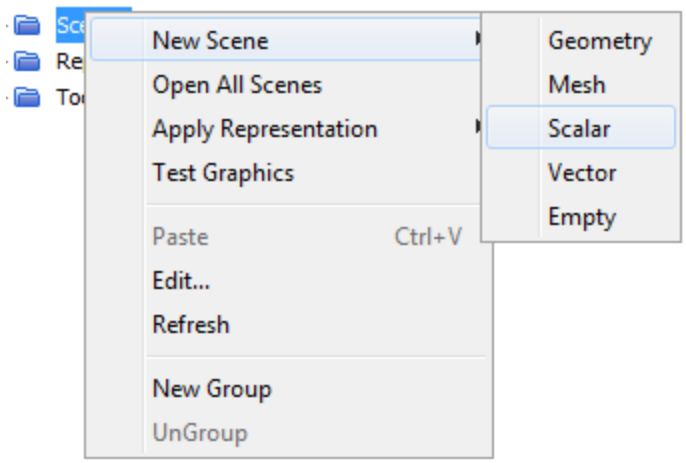

Fig. 22: Creating a scalar scene in Star CCM+. This can be done by right clicking the scalar folder shown on the left side of the Star CCM+ window.

Monitoring a scalar like velocity is easily done on a plane. A plane in the middle of the open area of the mold, showing parts of the fluid and porous regions, was created. Figure 23 shows this plane being created.

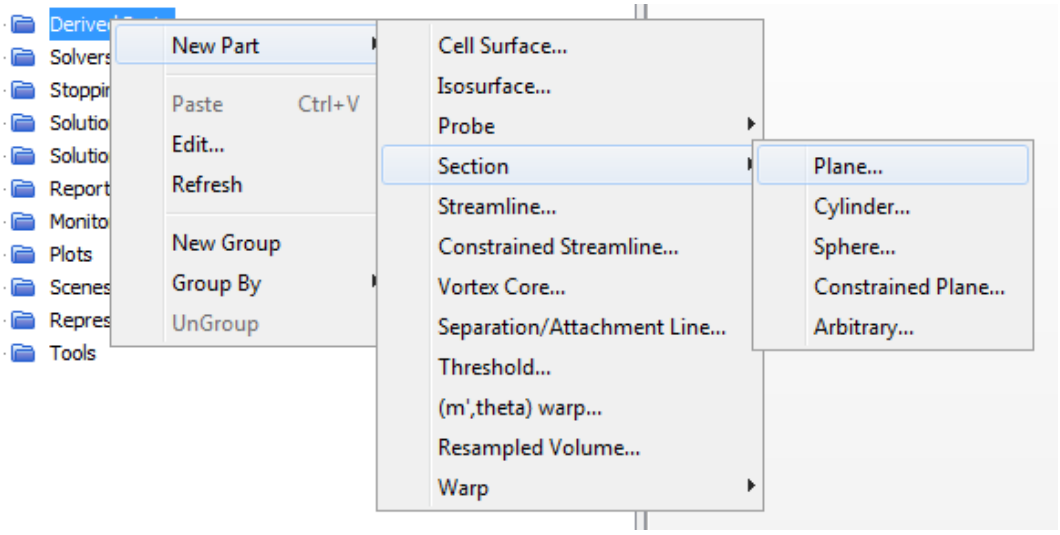

Fig. 23: Creating a plane in Star CCM+. This can be done by right clicking the "Derived Parts" folder shown on the left side of the Star CCM+ window. Then, the above menus can be accessed.

Star CCM+ defaults to placing the plane origin in the center of the geometry. The plane's origin and normal axis can be modified according to the preference of the modeler. Figure 24 shows the spatial coordinates used for simulations described in this section.

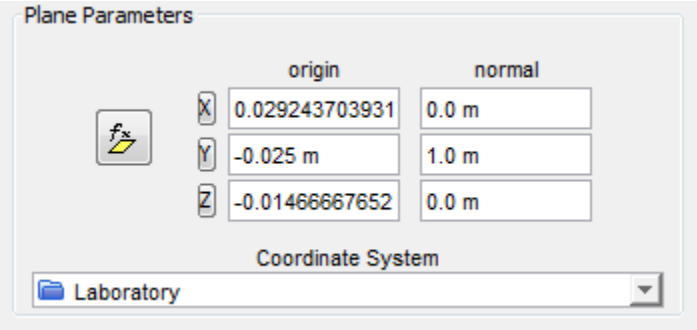

Fig. 24: Spatial coordinates and orientation of plane used to monitor fluid velocity.

The newly created plane was then selected as the part of interest in the scalar scene, shown in Figure 25. Velocity magnitude was then selected as the scalar of interest, shown in Figure 26.

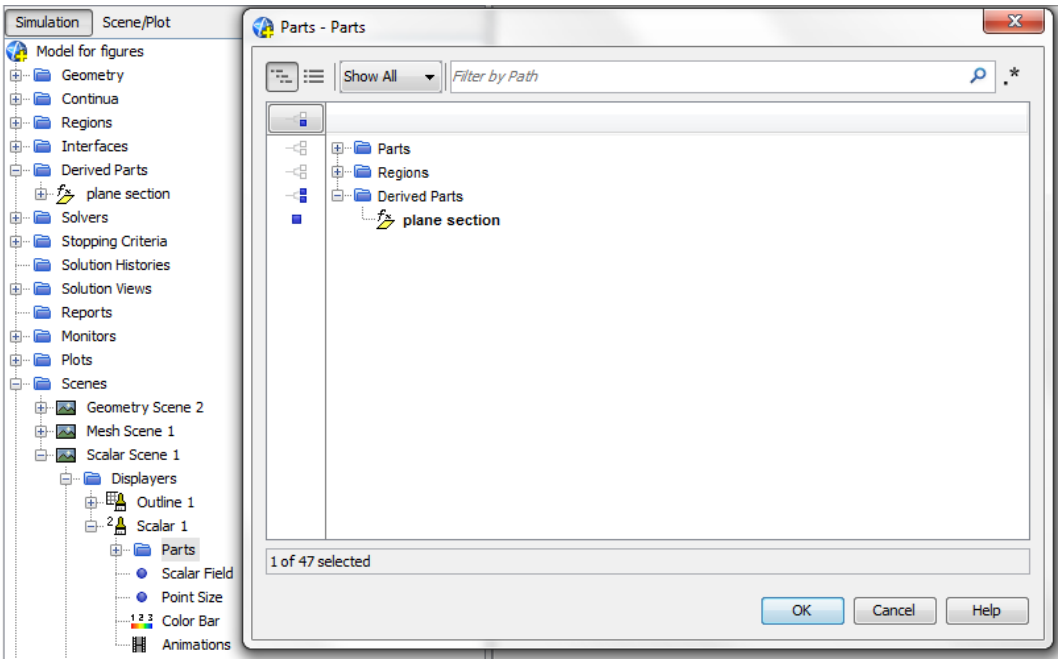

Fig. 25: Select plane for scalar scene display. This menu is available after double clicking the parts folder shown above.

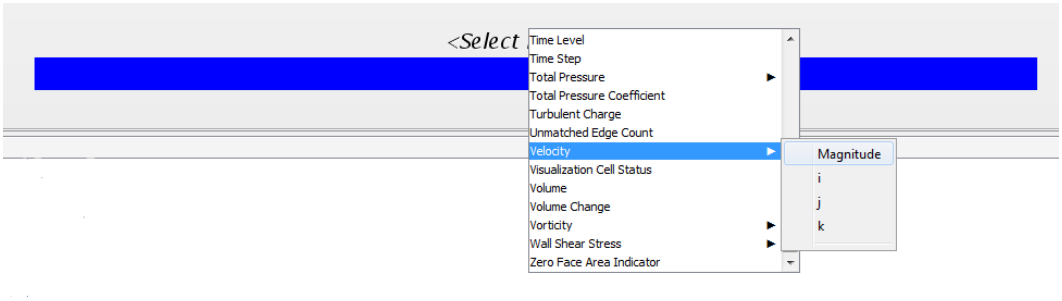

Fig. 26: Select velocity (magnitude) for scalar scene display by right clicking the blue bar found at the bottom of a newly created scalar scene.

3.2.6. Extracting Data from Completed Simulation

After simulations finished running, data were extracted and analyzed in Microsoft Excel. Data extraction begins with the creation of line probes, much like how a plane was created to visually monitor fluid velocity in a scalar scene, and can be configured to lie on a previously created plane. Figure 27 shows how to create a line probe. Probes used to extract data contained fifty points and ran vertically on the x-z plane. Figure 28 shows the

spatial coordinates of an example line probe. The location of the line can be varied to collect data from different positions on the plane.

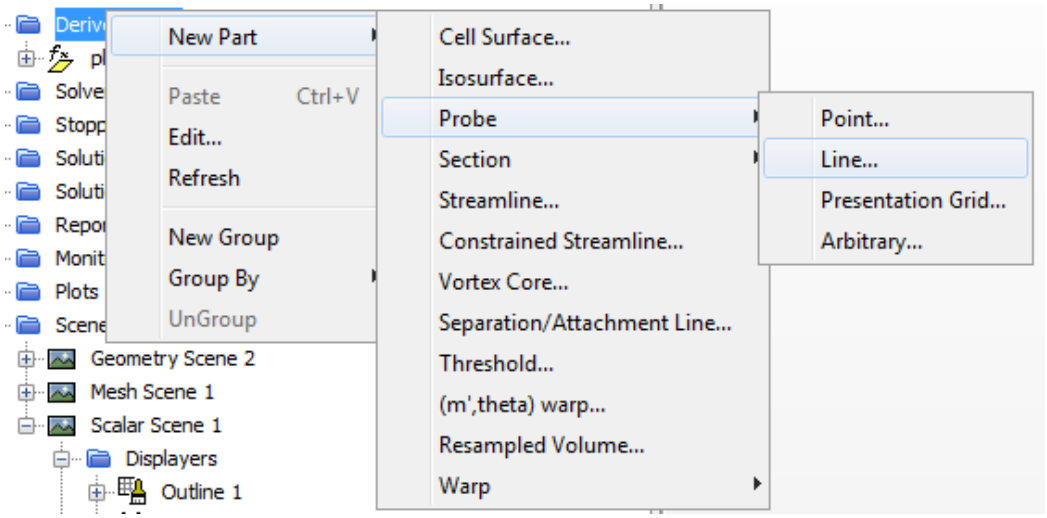

Fig. 27: Creating a line probe in Star CCM+. This can be done the same way a plane was created.

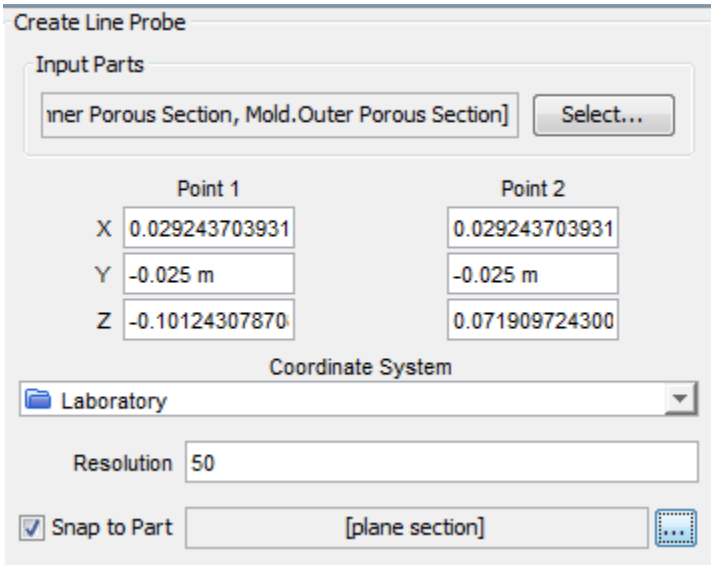

Fig. 28: Spatial coordinates of example line probe.

Data can be extracted from the line probes within Star CCM+ and exported as a comma separated value (CSV) file. A “XYZ Internal Table” was created to extract the data, done by right clicking the “tables” menu after opening the “Tools” dropdown menu.

Figure 29 shows how to create an internal table. A variety of scalars can be selected for extraction. Multiple line probes can be extracted as well. Scalar and part selection is shown for an example table in Figure 30. Figure 31 shows where to find the “extract” and “export” options.

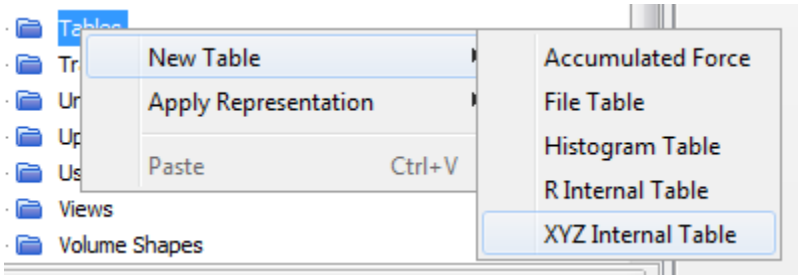

Fig. 29: Creating an internal table in Star CCM+. A table can be created by opening the “Tools” dropdown menu in the toolbar on the left side of the Star CCM+ window and right clicking the “Table” folder.

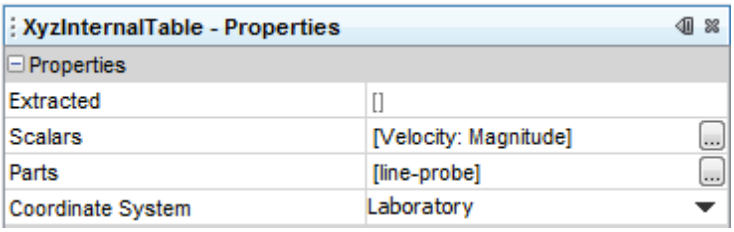

Fig. 30: Example table properties once parts and scalars are selected.

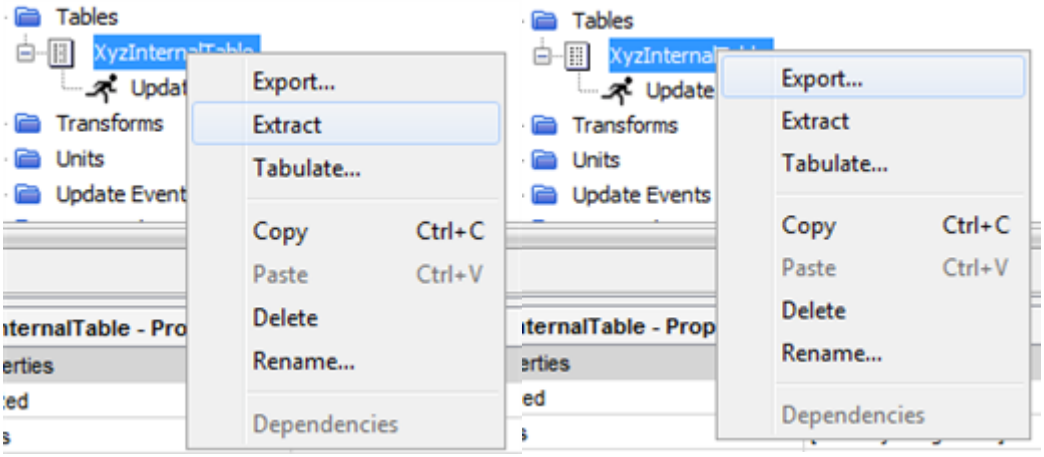

Fig. 31 Left: Extracting data from finished simulation. Right: Exporting data from table. These options are accessibly by right clicking the newly created table.

Methods outlined in this section were used to create simulations for each resin. Models were first run with lower resolution to confirm a correct setup before the number of cells was increased to the number included in this section. The same methodology could be used to model flow through molds with different arrangements of inlets and outlets, or different geometries altogether.

4. Results

The methodology outlined in Section 3 was used to generate a simulation for the one inlet-one outlet configuration. Results triggered interest in running a second simulation involving a two inlet-two outlet configuration. This section will present the results from both simulations and relate them to goals of the project.

4.1. One Inlet and One Outlet

Models were run to completion for simulations involving Resin A and Resin B. Before data analysis each model was checked for validity. A scalar scene for a cross section of the open mold area was generated to inspect fluid velocity for simulations of each resin. Residuals were also monitored. Figure 32 is an example residual plot taken from a simulation for Resin A illustrating a gradual decrease in residuals until stabilization. A velocity scene for the same simulation is contained in Figure 33.

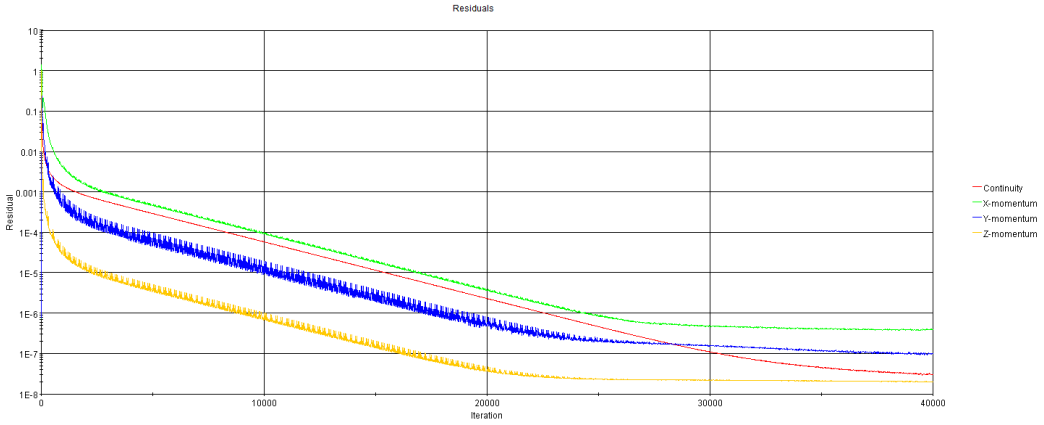

Fig. 32: Example residual plot for simulation of flow of Resin A through mold. Residuals gradually decreased until stabilization, indicative of a completed simulation.

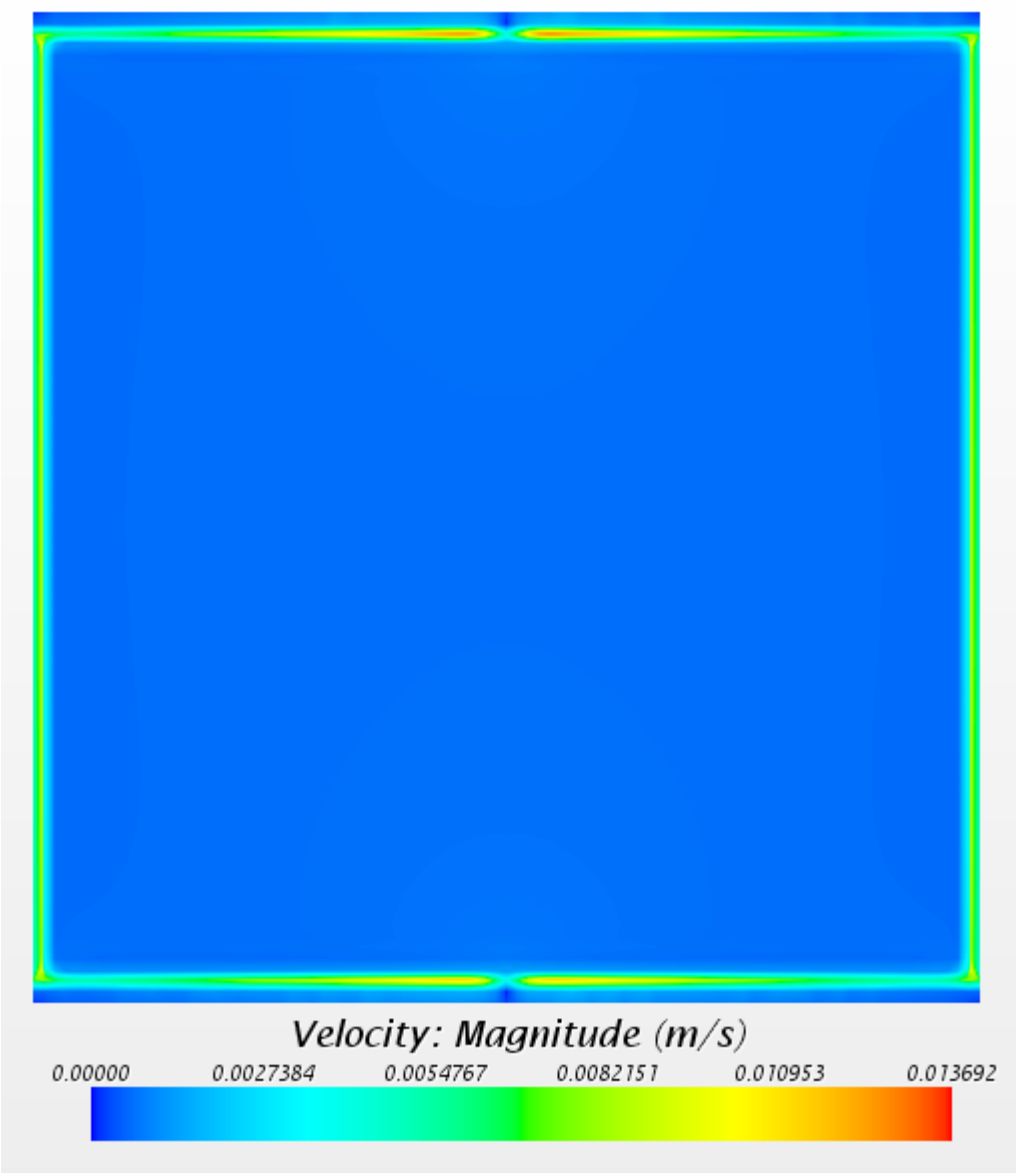

Fig. 33: Velocity magnitude for simulation of Resin A. Flow shown is in the XZ coordinate plane and flow direction is from the top to the bottom of the page.

Figures 32 and 33 are examples of quick checks performed on completed simulations to confirm that results were viable. By intuition, fluid velocity should be higher near the edges of the mold; completed simulations should reflect this. Fluid velocity is expected to be almost negligible in the mold plenums. Because the mold is symmetrical about its vertical axis, symmetry should also be visible in the results. Figure

33 shows both of these intuitions to be true. Brighter colors indicate higher fluid velocity, clearly visible around the edges of the mold. Plenums are located at the top and bottom of the mold and seen visually as the areas with low fluid velocity in the top and bottom of Figure 33.

Data were extracted from simulations after a model was validated in this manner. Localized fluid pressure was of particular interest, as an even pressure distribution along the x axis was desired to aid resin infusion. Figure 34 shows where line probes were created in each simulation for data extraction. The centerline of the XZ plane is located approximately at the vertical line $z = 1.15$ inches. Line probes were created symmetrically about the centerline with increasing density towards both edges of the mold.

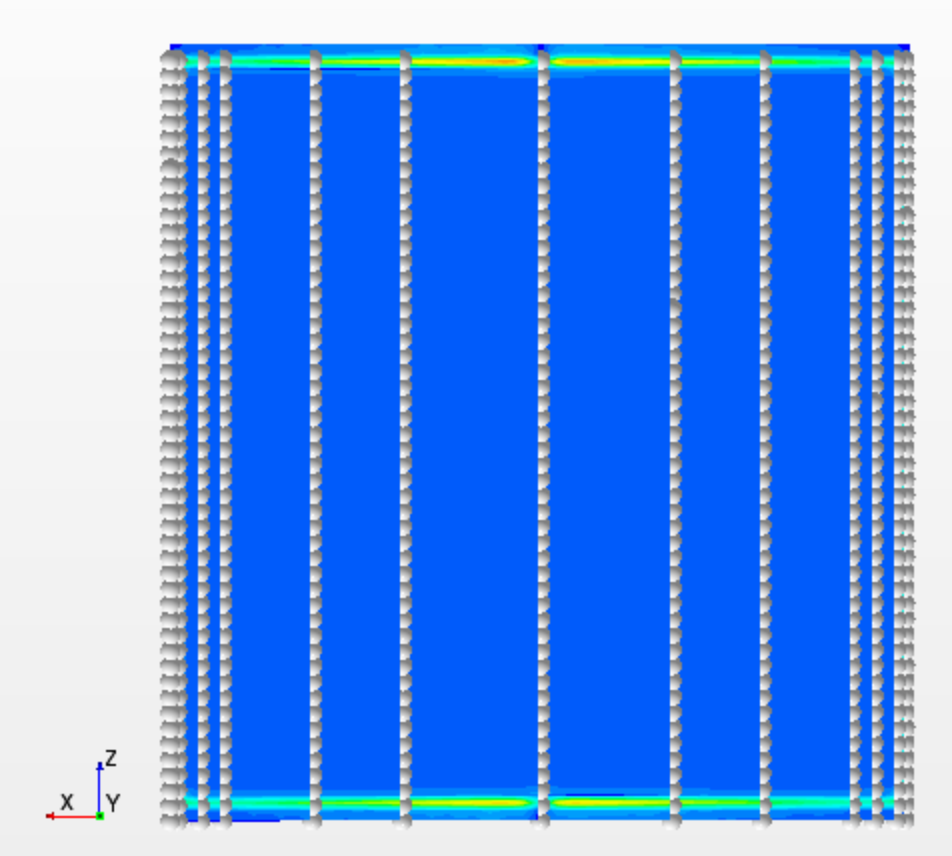

Fig. 34: Location of line probes on XZ plane. Lines are symmetrically distributed around the center axis of the mold and increase in density towards the mold edges. Each line has fifty points and will therefore extract fifty pressure values.

Absolute pressure values were extracted as a CSV file for manipulation in Microsoft Excel and MATLAB. Extracted CSV files automatically came with X, Y, and Z coordinates for each pressure value. The Y coordinates and column headings were removed from each CSV file in Excel. Data were also ordered vertically by their Z coordinates. The CSV files were then ready for importation into MATLAB.

MATLAB codes were written to generate figures for each set of pressure data. All scripts are contained in Appendix A. Two sets of data were imported for the one inlet one outlet mold configuration, one each for Resin A and Resin B. Data were fit with a polynomial function of the fifth order in X and Y [26, 27]. They were plotted with a

surface generated from the polynomial fit [26, 27]. Figure 35 was generated to display the absolute pressure on a horizontal plane through the open cavity of the mold for a simulation of Resin A.

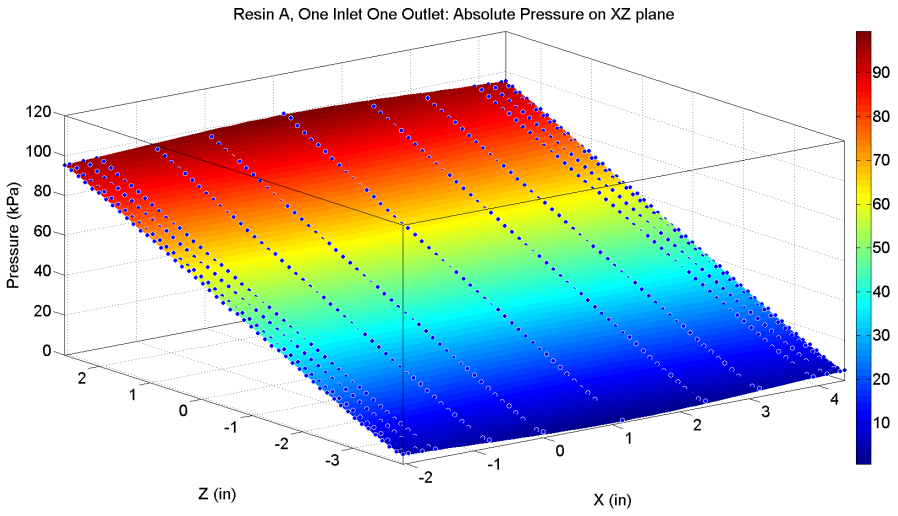

Fig. 35: Three dimensional plot of absolute pressure on the XZ plane for the simulation of flow of Resin A through a mold with one inlet and one outlet. Extracted data points are shown in blue, and the surface fit to the data is colored based on the pressure magnitude. X and Z coordinates are in inches (in); Absolute pressure is shown in kilo Pascals (kPA).

Visible in Figure 35 is slight curvature in the surface about a line parallel to the Z axis. To examine this behavior further, data were plotted for the upper and lower sections of the plane shown in Figure 35. Figures 36 and 37 contain these new figures.

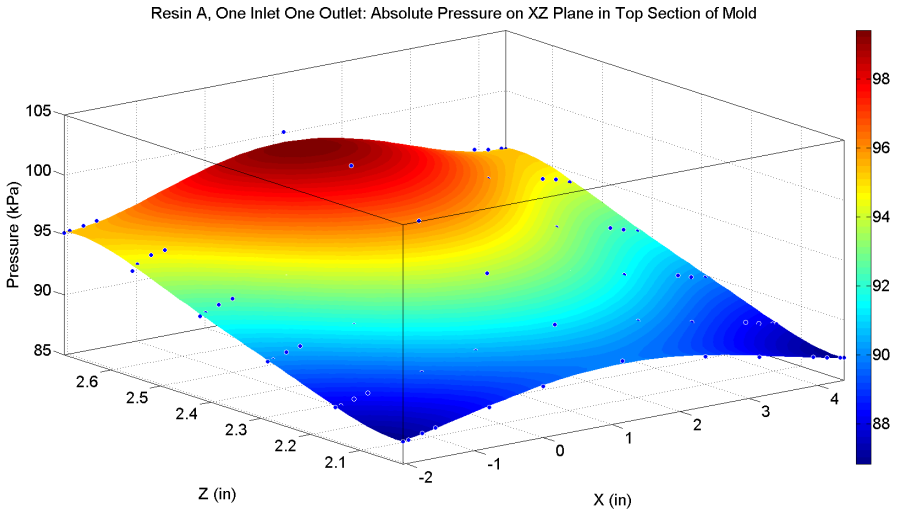

Fig. 36: Three dimensional plot of absolute pressure on the XZ plane for the simulation of flow of Resin A through the upper section of a mold with one inlet and one outlet. Extracted data points are shown in blue, and the surface fit to the data is colored based on the pressure magnitude. X and Z coordinates are in inches (in); Absolute pressure is shown in kilo Pascals (kPA).

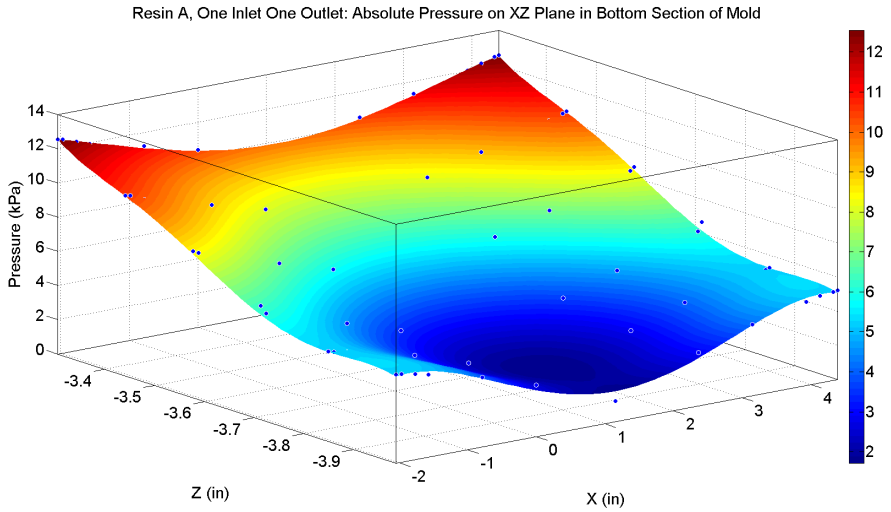

Fig. 37: Three dimensional plot of absolute pressure on the XZ plane for the simulation of flow of Resin A through the lower section of a mold with one inlet and one outlet. Extracted data points are shown in blue, and the surface fit to the data is colored based on the pressure magnitude. X and Z coordinates are in inches (in); Absolute pressure is shown in kilo Pascals (kPA).

Curvature in the data is very apparent in Figures 36 and 37. Absolute pressure is greatest in the middle of the mold in the upper region of the open area, whereas in the

lower region of the mold the absolute pressure is greatest along the edges. This trend is also seen for simulations of Resin B. Figure 38 shows the absolute pressure on a horizontal plane through the open cavity of the mold for a simulation of Resin B. Figures 39 and 40 were generated to enlarge curvature visible in the data.

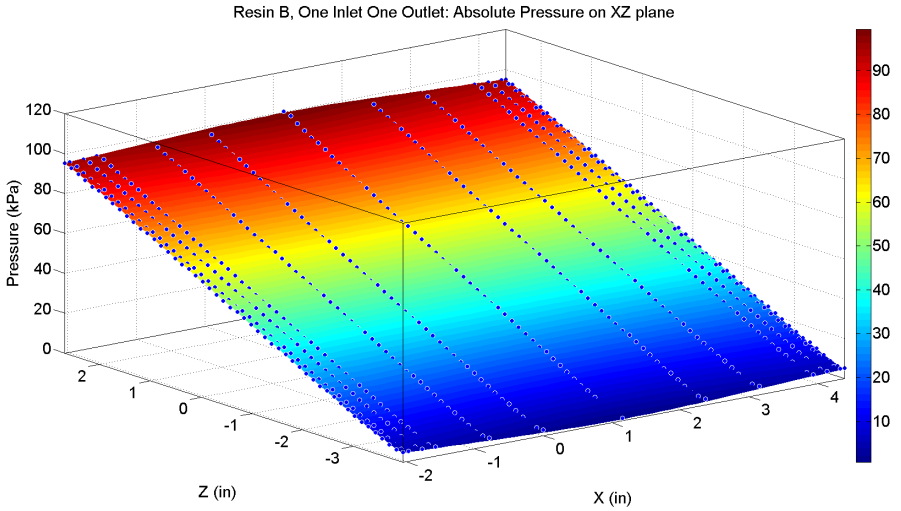

Fig. 38: Three dimensional plot of absolute pressure on the XZ plane for the simulation of flow of Resin B through a mold with one inlet and one outlet. Extracted data points are shown in blue, and the surface fit to the data is colored based on the pressure magnitude. X and Z coordinates are in inches (in); Absolute pressure is shown in kilo Pascals (kPA).

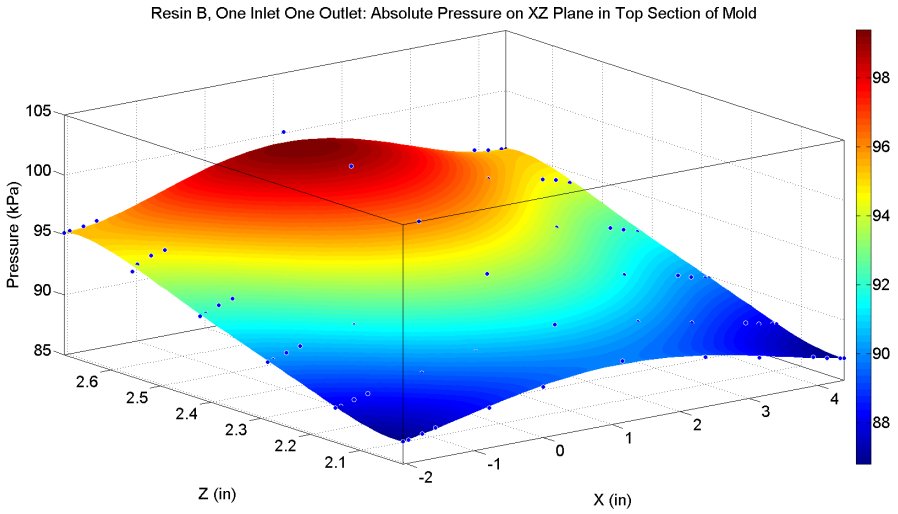

Fig. 39: Three dimensional plot of absolute pressure on the XZ plane for the simulation of flow of Resin B through the upper section of a mold with one inlet and one outlet. Extracted data points are shown in blue, and the surface fit to the data is colored based on the pressure magnitude. X and Z coordinates are in inches (in); Absolute pressure is shown in kilo Pascals (kPA).

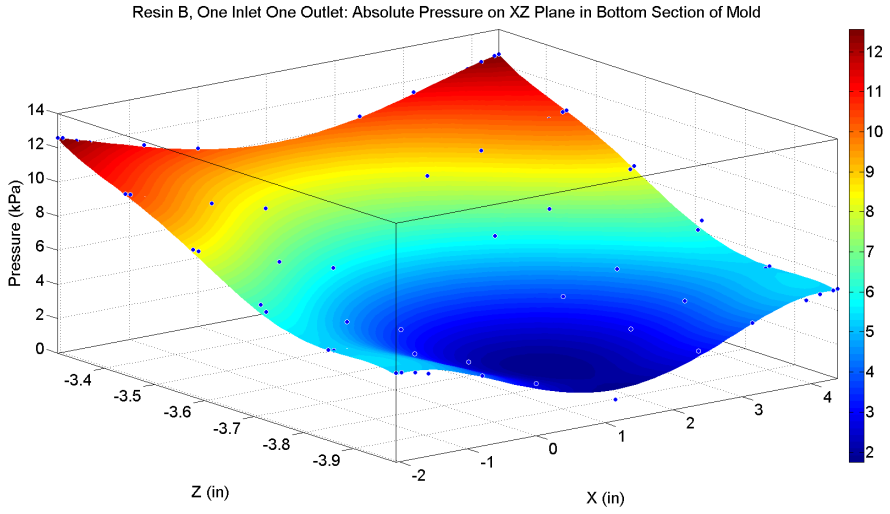

Fig. 40: Three dimensional plot of absolute pressure on the XZ plane for the simulation of flow of Resin B through the lower section of a mold with one inlet and one outlet. Extracted data points are shown in blue, and the surface fit to the data is colored based on the pressure magnitude. X and Z coordinates are in inches (in); Absolute pressure is shown in kilo Pascals (kPA).

A comparison of the absolute pressures associated with each resin reveals a large amount of similarity between the two simulations. A closer inspection of the two absolute

pressure plots for the lower regions of the open cavity of the mold, Figures 37 and 40, shows that the pressure change between the centerline and edges of the mold was greater for Resin B.

4.2.Two Inlets and Two Outlets

Results from the simulations with one inlet and one outlet port prompted an investigation into how mold geometry affects pressure distribution about the mold's central axis. Mold geometry was modified to include another inlet-outlet pair, bringing the total to two each. This geometry is shown in Figure 41. Inlet and outlet diameters were not modified and the inlets and outlets were evenly spaced around the centerline of the mold. Simulations were created for Resin A and Resin B following the methodology described in Section 3 and run to completion.

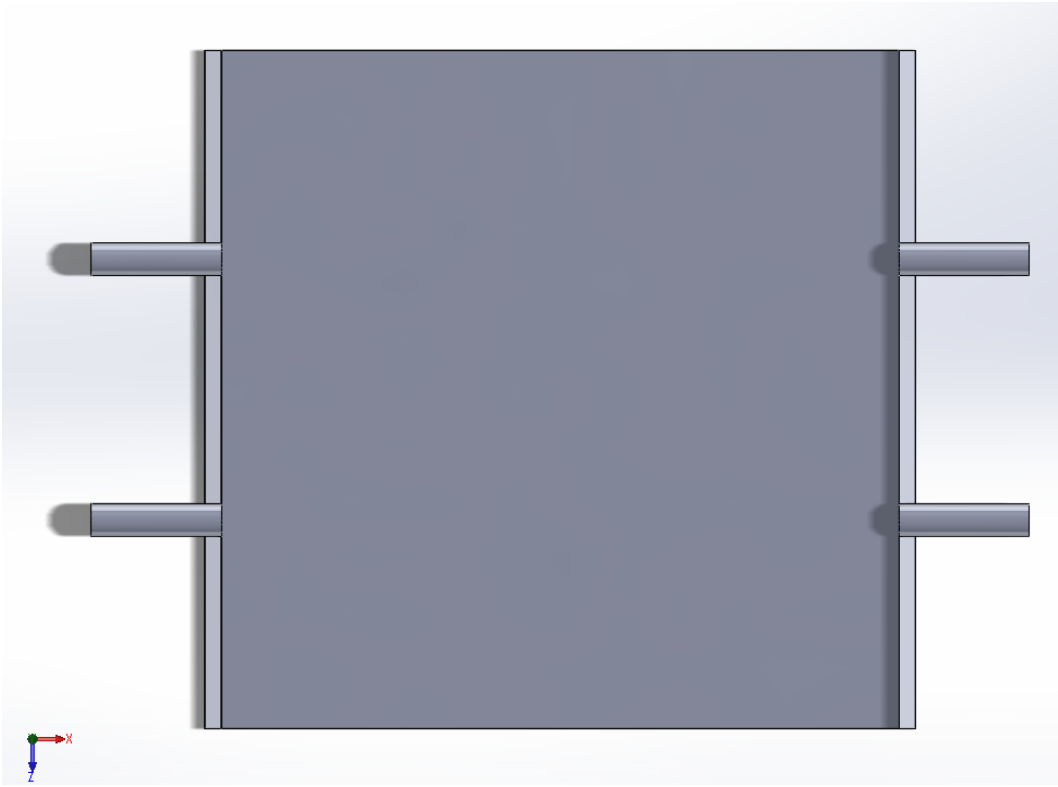

Fig, 41: Geometry of proposed mold with two inlets and two outlets.

Absolute pressure in the XZ plane was again of interest. Line probes were created for data extraction in the same locations as those used for simulations in Section 4.1. Figures were created to examine the spatial distribution of pressure within the open area of the mold using the same method as that used for simulations with one inlet and one outlet. Figures 42 through 44 display the pressure distribution for the simulation of the flow of Resin A through a mold with two inlets and two outlets.

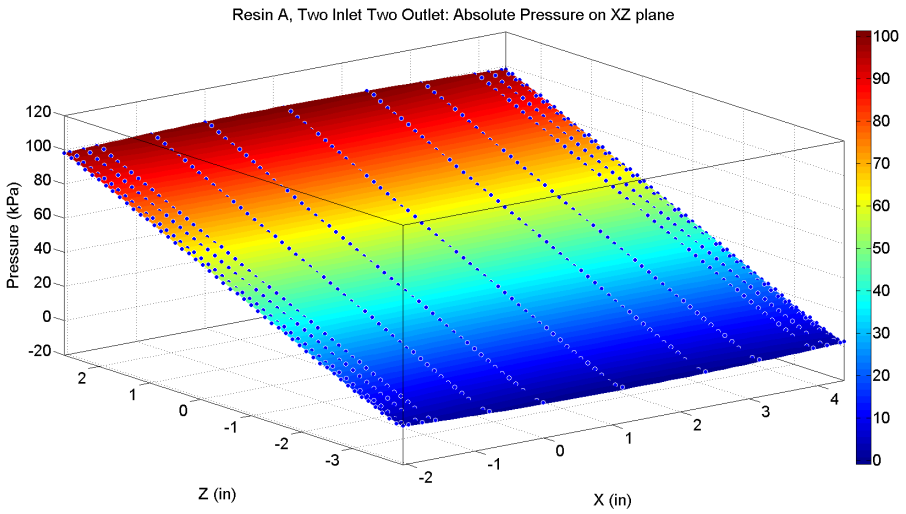

Fig. 42: Three dimensional plot of absolute pressure on the XZ plane for the simulation of flow of Resin A through a mold with two inlets and two outlets. Extracted data points are shown in blue, and the surface fit to the data is colored based on the pressure magnitude. X and Z coordinates are in inches (in); Absolute pressure is shown in kilo Pascals (kPA).

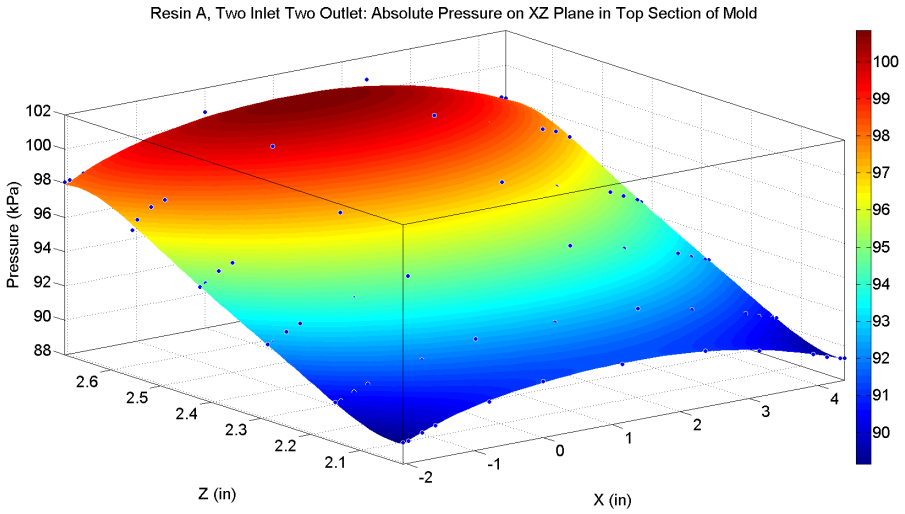

Fig. 43: Three dimensional plot of absolute pressure on the XZ plane for the simulation of flow of Resin A through the upper section of a mold with two inlets and two outlets. Extracted data points are shown in blue, and the surface fit to the data is colored based on the pressure magnitude. X and Z coordinates are in inches (in); Absolute pressure is shown in kilo Pascals (kPA).

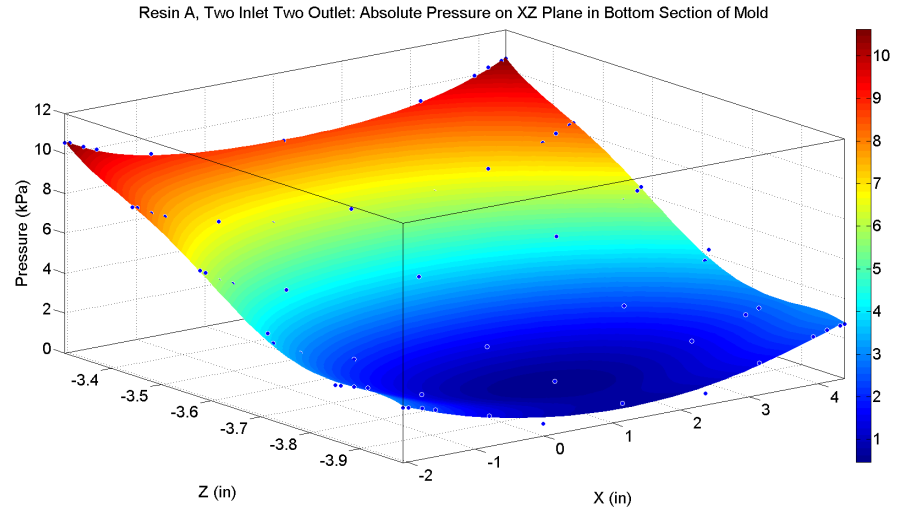

Fig. 44: Three dimensional plot of absolute pressure on the XZ plane for the simulation of flow of Resin A through the lower section of a mold with two inlets and two outlets. Extracted data points are shown in blue, and the surface fit to the data is colored based on the pressure magnitude. X and Z coordinates are in inches (in); Absolute pressure is shown in kilo Pascals (kPA).

The pressure distribution through the mold with two inlets and two outlets involving Resin A is very similar to the distribution through the corresponding simulation

of the mold with one inlet and one outlet. There is still curvature present throughout the open section of the mold. However, the pressure gradient between the edge and center of the mold is less severe, as seen in a comparison of Figures 37 and 44. Results from the simulation of Resin B flowing through the new geometry are shown in Figures 45 through 47.

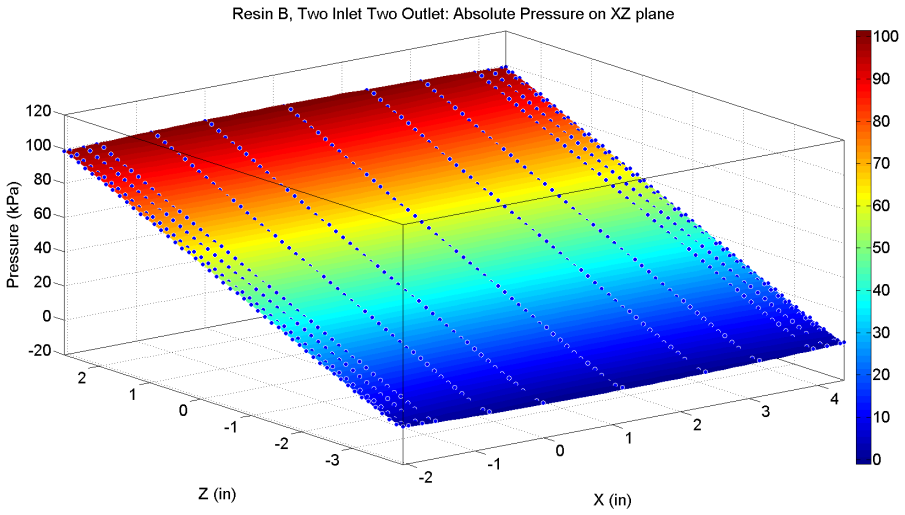

Fig. 45: Three dimensional plot of absolute pressure on the XZ plane for the simulation of flow of Resin B through a mold with two inlets and two outlets. Extracted data points are shown in blue, and the surface fit to the data is colored based on the pressure magnitude. X and Z coordinates are in inches (in); Absolute pressure is shown in kilo Pascals (kPA).

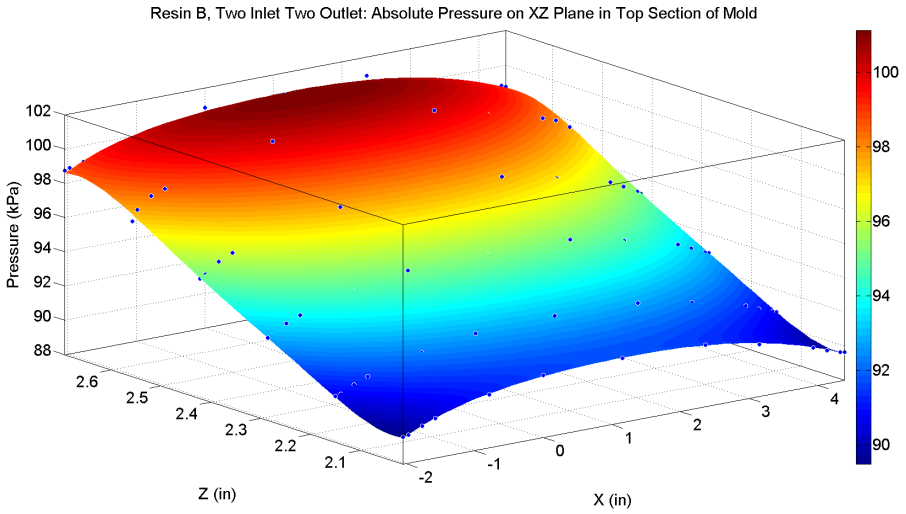

Fig. 46: Three dimensional plot of absolute pressure on the XZ plane for the simulation of flow of Resin B through the upper section of a mold with two inlets and two outlets. Extracted data points are shown in blue, and the surface fit to the data is colored based on the pressure magnitude. X and Z coordinates are in inches (in); Absolute pressure is shown in kilo Pascals (kPA).

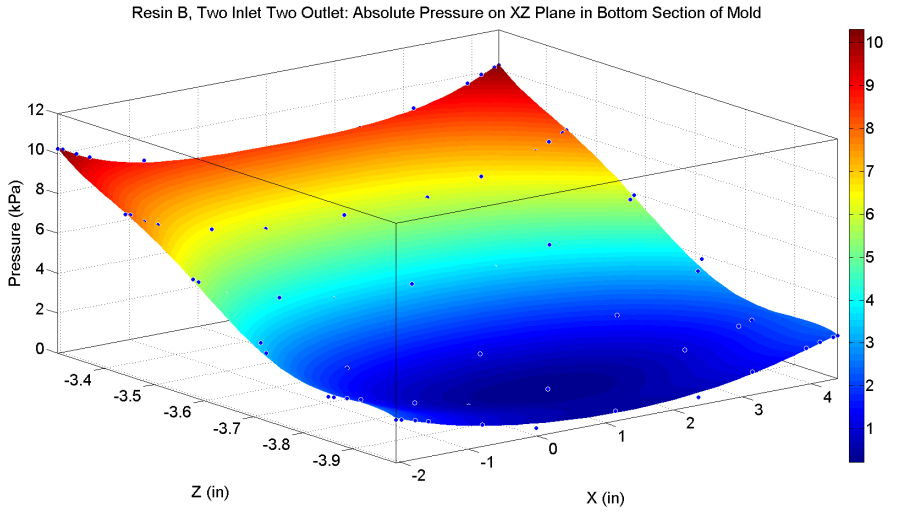

Fig. 47: Three dimensional plot of absolute pressure on the XZ plane for the simulation of flow of Resin **A** through the lower section of a mold with two inlets and two outlets. Extracted data points are shown in blue, and the surface fit to the data is colored based on the pressure magnitude. X and Z coordinates are in inches (in); Absolute pressure is shown in kilo Pascals (kPA).

The same trend is shown in Figures 44 through 47. A lower pressure gradient between the edge and center of the mold is shown especially in Figure 47, easily seen

when compared to Figure 40. Results from simulations of flow through a mold with two inlets and two outlets suggest that a much more even horizontal pressure distribution can be achieved in the XZ plane than that observed for the one inlet, one outlet simulations.

5. Conclusion

As sustainability becomes a more and more important driver for global change, the environmental impact of everyday actions and items is scrutinized. Sustainability is no longer limited to the energy industry; the manufacturing and industrial sectors have realized the economic potential of going green.

Sandwich structures utilize a lightweight core coupled with thin, stiff sheets to increase bending strength and stiffness while maintaining a low density. Ecovative is a manufacturer that has developed a Styrofoam-like material whose primary ingredient is fungal mycelia. The material is one hundred percent biodegradable. It is therefore a good candidate to be the core of a sandwich structure.

This thesis examined resin infusion of carbon fiber mats to be used in conjunction with a mycelia-based core to create a sandwich structure. The theoretical background, methodology, and analysis of CFD simulations created in Star CCM+ was presented. Section 2 presented the fundamental fluid dynamics governing viscous fluid flow through porous media, starting with the continuity equation and the Navier-Stokes equation. The general workflow of modeling in Star CCM+ was reviewed. Darcy's law and its application in Star CCM+ was then presented. Two methods of modeling porous media were discussed: modeling a porous solid as a porous region and modeling porous media with porous baffle interfaces. Modeling considerations specific to vacuum media were reviewed and an overview of experimental treatment of porous media followed.

The methodology used to create simulations for this thesis was discussed in detail in Section 3. The importation of CAD geometry, discretization of modeling regions, and the selection of meshing and physics models was covered. The configuration of a

simulation to model porous media was explicitly documented. Running a simulation in Star CCM+ and extraction of results was then covered. Attention was paid in particular to verifying simulation results.

Section 4 contained simulation results pertinent to this thesis. The procedure of data extraction specific to this work was reviewed, followed by documentation of data analysis. Plots of absolute pressure within the mold cavity for simulations of both resins and two different model geometries were presented. Implications of the results were discussed.

This thesis is intended to serve as a model for modeling porous media in Star CCM+ and documentation of modeling efforts to date. Future work will involve the modeling of more complex mold geometries. A similar methodology can be used to model the resin infusion of outer layers of a mycelia core to investigate the potential of creating a sandwich structure from mycelia alone.

References

1. United States Environmental Protection Agency. Executive Report, Inventory of U.S. Greenhouse Gas Emissions and Sinks. (Accessed October 22, 2014) (PDF).
2. Energy Information Agency. Annual Energy Outlook 2014. (Accessed October 22, 2014) (PDF).
3. United States Department of State. U.S. Climate Action Report 2010. Washington: Global Publishing Services, June 2010. (Accessed October 22, 2014) (PDF).
4. MIT Sloan Management Review and Boston Consulting Group. Sustainability Nears a Tipping Point. (Accessed October 22, 2014) (PDF).
5. International Union for Conservation of Nature. Future of Sustainability. (Accessed October 22, 2014) (PDF).
6. Gunther, Marc. The Guardian. Can Mushrooms Replace Plastic? http://www.theguardian.com/sustainable-business/mushrooms-new-plastic-ecovative. (Accessed October 3, 2014).
7. Frazier, Ian. The New Yorker. Form and Fungus. http://www.newyorker.com/magazine/2013/05/20/form-and-fungus. (Accessed October 3, 2014).
8. Mushroom Materials. Ecovative. http://www.ecovativedesign.com/mushroom-materials/. (Accessed October 3, 2014).
9. Products and Applications. Ecovative. http://www.ecovativedesign.com/products-and-applications/. (Accessed October 3, 2014).
10. Petras, Achilles. Design of Sandwich Structures. Ph.D. Dissertation, Cambridge University, Cambridge, UK. (Accessed November 18, 2014) (PDF).
11. Fibreglast. Vacuum Infusion – The Equipment and Process of Resin Infusion. (Accessed October 6, 2014) (PDF).
12. Datta, Sujit S. Getting out of a tight spot: The physics of fluid flow through porous materials. Ph.D. Dissertation, Harvard University, Cambridge, MA. (Accessed October 25, 2014) (PDF).
13. Wei, M. Ground Water Resources of British Columbia, Chapter 2 – Origin, Occurrence, and Movement of Ground Water. http://www.env.gov.bc.ca/wsd/plan_protect_sustain/groundwater/gwbc/C02_origin.html (Accessed November 11, 2014).
14. Koivu, Viivi. Analysis Of Fluid Flow Through Porous Media Based On X-Ray Micro-Tomographic Reconstructions. Ph.D. Dissertation, University of Jyväskylä, Jyväskylä, Finland, 2010 (PDF).
15. Compass Tdyn Documentation. Flow through porous materials. (Accessed October 27, 2014) (PDF).
16. Star CCM+ Documentation. Specifying Porosity. (Accessed November 10, 2014) (PDF).
17. Star CCM+ Documentation. Isotropic Resistance Using the Ergun Equation (Forchheimer for Packed Beds). (Accessed November 10, 2014) (PDF).
18. George, A. Optimization of Resin Infusion Processing for Composite Materials: Simulation and Characterization Strategies. Ph.D. Dissertation, University of Stuttgart, Stuttgart, Germany, 2011 (PDF).

19. Song, X. Vacuum Assisted Resin Transfer Molding (VARTM): Model Development and Verification. Ph.D. Dissertation, Virginia Polytechnic Institute and State University, Blacksburg, VA, 2003 (PDF).
20. Star CCM+ Documentation. Porous Baffle Interface. (Accessed October 26, 2014).
21. Macdonald, I. F. et al, Flow through porous media – the Ergun equation revisited. (Accessed October 27, 2014) (PDF).
22. Star CCM+ Tutorial Guide. Porous Resistance: Isotropic Media. (Accessed October 27, 2014) (PDF).
23. Rizzolo, Robert. Rennselaer Polytechnic Institute. Written Communication, 2014
24. Rizzolo, Robert. Rennselaer Polytechnic Institute. Oral Communication, 2014
25. Properties of Liquids (Reference 135). Watlow. (Accessed January 26, 2015) (PDF).
26. MATLAB Documentation. Fit Curve or Surface to Data. (Accessed February 13, 2015).
27. Boston University ITS. Using MATLAB to Visualize Scientific Data. (Accessed February 13, 2015).
28. Star CCM+, version 9.0.4; Computational Fluid Dynamics Package: CD-Adapco. (Accessed October 22, 2014).
29. MATLAB, version R2012b; Technical Computing Software: Mathworks. (Accessed February 13, 2015).
30. SolidWorks 2014 x64 edition; Dassault Systems. (Accessed October 22, 2014).

Appendix

Appendix A: Matlab Scripts for Figure Generation

Script for Analysis of Resin A: One inlet, One outlet. The same script was used to generate figures for each simulation; only the imported file name was changed. The script below is commented specifically for Resin A: One inlet One Outlet.

```
%One inlet One outlet
%Resin A

clear all
close all
clc

%Import Data and separate into columns

C=csvread('ResinA_pressuredata.csv');
x=C(:,1); %x coordinate
y=C(:,2); %z coordinate
z=C(:,3); %pressure
x=x*39.3701; %convert to inches
y=y*39.3701; %convert to inches
z=z/1000; %convert to kPa

%Fit a 5th degree polynomial function in x and y to the data

z_fit=fit( [x, y], z, 'Poly55');

%Separate data into smaller subsections

%bottom section
x1=x(1:13*6);
y1=y(1:13*6);
z1=z(1:13*6);

%top section
x2=x(end - 13*6 + 1:end);
y2=y(end - 13*6 + 1:end);
z2=z(end - 13*6 + 1:end);

%Fit a 5th degree polynomial function in x and y to the data
subsections

z1_fit=fit( [x1, y1], z1, 'Poly55');
z2_fit=fit( [x2, y2], z2, 'Poly55');

%Plot imported data and surface fit to data from generated polynomial
%functions
```

```
figure
plot(z_fit, [x,y], z); zoom on; rotate3d on; hold on;
shading interp; colorbar vertical;
title('Resin A, One inlet One Outlet: Absolute Pressure on XZ plane');
xlabel('X (in)');ylabel('Z (in)');zlabel('Pressure (kPa)');
set(gca,'fontSize',22);
set(findall(gcf,'type','text'),'fontSize',22);

figure
plot(z1_fit, [x1,y1], z1); zoom on; rotate3d on; hold on;
shading interp; colorbar vertical;
title('Resin A, One inlet One Outlet: Absolute Pressure on XZ Plane in
Bottom Section of Mold');
xlabel('X (in)');ylabel('Z (in)');zlabel('Pressure (kPa)');
set(gca,'fontSize',22);
set(findall(gcf,'type','text'),'fontSize',22);

figure
plot(z2_fit, [x2,y2], z2); zoom on; rotate3d on; hold on;
shading interp; colorbar vertical;
title('Resin A, One inlet One Outlet: Absolute Pressure on XZ Plane in
Top Section of Mold');
xlabel('X (in)');ylabel('Z (in)');zlabel('Pressure (kPa)');
set(gca,'fontSize',22);
set(findall(gcf,'type','text'),'fontSize',22);
```